Extracting ore-deposit-controlling structures from aeromagnetic, gravimetric, topographic, and regional geologic data in western Yukon and eastern Alaska

Matías G. Sánchez[1], Murray M. Allan[1], Craig J. R. Hart[1], and James K. Mortensen[1]

Abstract

Aeromagnetic lineaments interpreted from reduced-to-pole (RTP) magnetic grids were compared with gravity, topography, and field-based geologic maps to infer regional structural controls on hydrothermal mineral occurrences in a poorly exposed portion of the North American Cordillera in western Yukon and eastern Alaska. High-frequency and variable-intensity aeromagnetic lineaments corresponding to discontinuities with an aeromagnetic domain change were interpreted as steep-dipping and either magnetite-destructive or magnetite-additive faults. These structures were interpreted to be predominantly Cretaceous in age and to have formed after the collision of the Intermontane terranes with the ancient Pacific margin of North America. To demonstrate the reliability of the aeromagnetic interpretation, we developed a multidata set stacking methodology that assigns numeric values to individual lineaments depending on whether they can be traced in residuals and first vertical derivative of RTP aeromagnetic grids, isostatic residual gravity grids, digital topography, and regional geologic maps. The sum of all numeric values was used to estimate the likelihood of the aeromagnetic lineament as a true geologic fault. Fault systems were interpreted from zones of lineaments with high spatial density. Using this procedure, 10 major northwest-trending fault systems were recognized. These were oriented subparallel to the regional Cordilleran deformation fabric, the mid-Cretaceous Dawson Range magmatic arc, and well-established crustal-scale dextral strike-slip fault systems in the area. These orogen-parallel fault systems were interpreted to play a structural role in the emplacement of known porphyry Cu-Au and epithermal Au systems of mid-Cretaceous (115–98 Ma) and Late Cretaceous (79–72 Ma) age. The procedure also identified seven northeast-trending, orogen-perpendicular fault-fracture systems that are prominent in eastern Alaska and exhibit sinistral-to-oblique extensional kinematics. These structures were interpreted to govern the emplacement of Late Cretaceous (72–67 Ma) porphyry Mo- and Ag-rich polymetallic vein and carbonate replacement systems in the region.

Introduction

Geophysical targeting is an invaluable mineral exploration tool in regions of poor rock exposure and limited geologic knowledge such as the unglaciated region of the western Yukon and eastern Alaska Cordillera. This region is composed of assembled crustal fragments of the Intermontane terranes, which are highly prospective to host mineral deposits (Allan et al., 2013; Nelson et al., 2013). However, the high proportion of colluvial and vegetation cover provides only limited rock exposures, which makes geologic and structural mapping a significant challenge (Figure 1). To increase the understanding of the regional geology and to enhance mineral exploration decision-making, we carried out a regional-scale structural interpretation that integrates aeromagnetic, gravity, topographic, and geologic data sets (Figures 2 and 3).

Airborne magnetic surveys constitute one of the most widely used geophysical techniques for mineral exploration and geologic interpretation (e.g., Roberts and Hudson, 1983; Grant, 1985; Gunn and Dentith, 1997; Hoschke, 2001; Nabighian et al., 2005; Purucker and Clark, 2011; Anderson et al., 2013; Shah et al., 2013), particularly in regions with poor bedrock exposure (Gunn et al., 1997; Logan et al., 2010). Specific examples of its applications to western North American geology and structure include: (1) the mapping of strong magnetic anomalies caused by buried basement and cratonic structures (Crawford et al., 2010), (2) analysis of weak signals assigned to Laurentian

[1]The University of British Columbia, Mineral Deposit Research Unit, Main Mall, Vancouver, British Columbia, Canada. E-mail: matsanch@gmail.com; mallan@eos.ubc.ca; chart@eos.ubc.ca; jmortensen@eos.ubc.ca.

Manuscript received by the Editor 19 May 2014; revised manuscript received 6 July 2014; published online 15 October 2014; corrected version published online 24 October 2014. This paper appears in *Interpretation*, Vol. 2, No. 4 (November 2014); p. SJ75–SJ102, 15 FIGS.
http://dx.doi.org/10.1190/INT-2014-0104.1.

margin sedimentary basins (Lund, 2008), (3) mapping of high-amplitude anomalies caused by buried Early Proterozoic magmatic arcs (Pilkington and Saltus, 2009), and (4) mineral exploration applications including structural controls of Mesoproterozoic massive sulfide and intrusion- and fault-related Ag-Pb-Zn and Cu-Ag veins, as well as control of Mesozoic lode gold and stratabound Cu-Ag deposits (McMechan, 2012). These and other applied magnetics studies have contributed substantially to the understanding of western North American crustal structure and tectonic evolution (e.g., Pilkington et al., 2006; Saltus, 2007; Nelson et al., 2013).

Aeromagnetic lineaments have long been used as a guide to regional structural controls on mineralization within metallogenic provinces of diverse geologic settings (e.g., Domzalski, 1966; Henley and Adams, 1992; Clark, 1999; Richards, 2000; Hildenbrand et al., 2001; Clark et al., 2004; Sandrin et al., 2007). In this study, linear and mainly magnetite-destructive discontinuities associated with aeromagnetic structural domain changes are interpreted to result from steep-dipping structures that may provide structural control of hydrothermal mineralization in the study area (Figure 4; Sánchez et al., 2013). The geologic and structural interpretation of the RTP magnetic grid and data enhancement filters constitutes the foundation of this study. Aeromagnetic data are used as a base layer for geologic and structural interpretation as they stand as the only available contiguous data set that conveys physical information about geologic units and structural features at a scale appropriate for regional targeting. By comparing the outputs of the aeromagnetic interpretations to many different data layers, including gravity, topography, and geologic maps, aeromagnetic lineaments (and specifically discontinuities) can be increasingly validated as being "true" geologic faults.

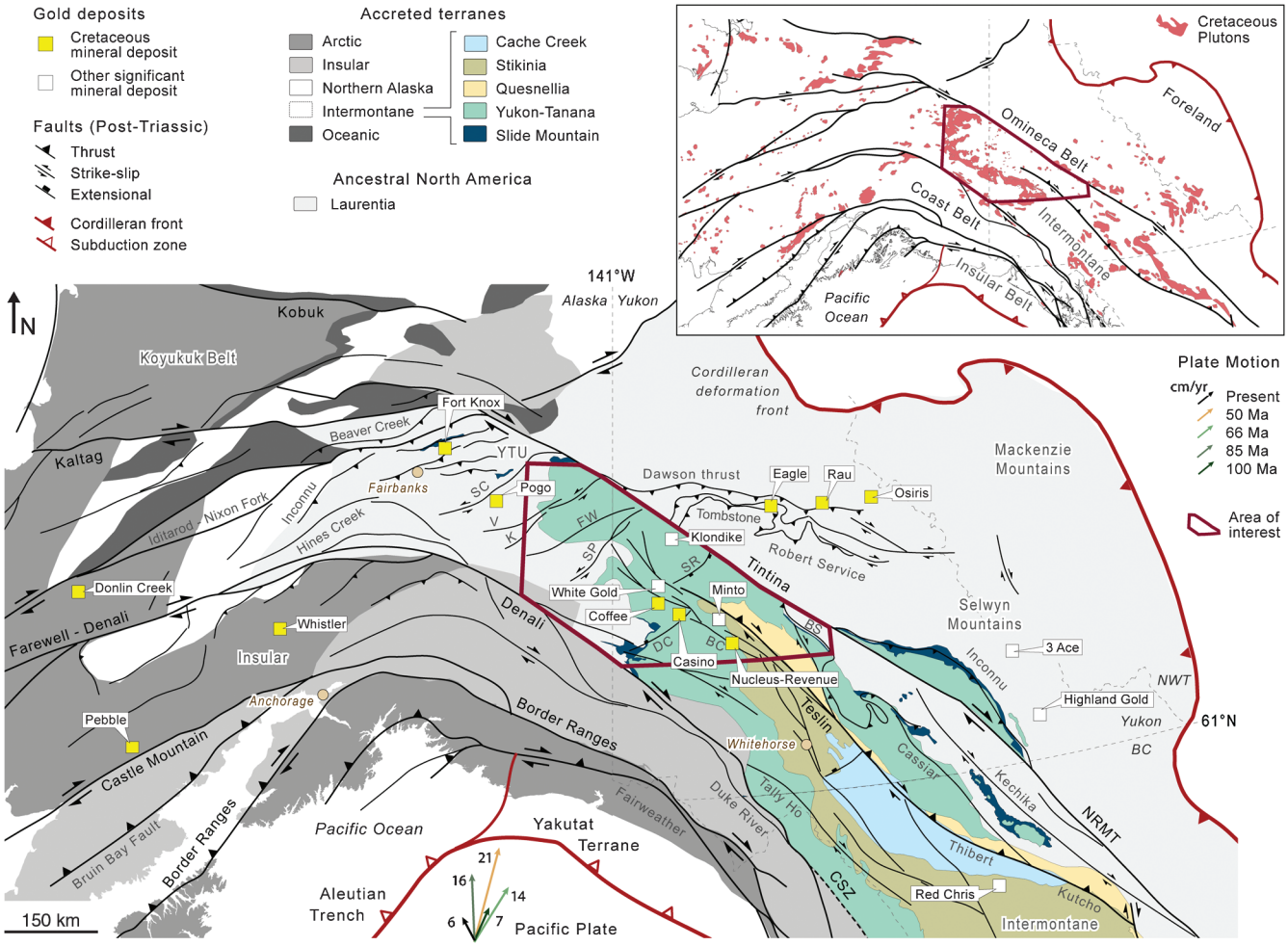

Figure 1. Tectonic map of the North American Cordillera showing major tectonic boundaries (after Colpron and Nelson, 2011), Mesozoic and Cenozoic faults, and main gold deposits. Fault abbreviations: SC = Shaw Creek, V = Volkmar, K = Kechumstuk, FW = Fortymile-Wolf Creek, SP = Sixtymile-Pika, SR = Stewart River, DC = Dip Creek, BC = Big Creek, CSZ = Coastal Shear Zone, BS = Big Salmon, and YTU = Yukon-Tanana Uplands. Relative plate motion vectors after Plafker and Berg (1994). The area of study is indicated by the red polygon. Inset shows Cretaceous plutons (after Hart et al., 2004a) and morphologic belts (after Gabrielse et al., 1991).

Tectonic and geologic framework

The magnetic data set used for this structural interpretation covers the Intermontane terranes of the North American Cordillera of western Yukon and eastern Alaska, flanked by the Tintina and Denali faults — two continental-scale dextral strike-slip faults that each accommodated >400 km of displacement in the early Cenozoic (Figure 1; Gabrielse et al., 2006). The Intermontane terranes represent an assemblage of now-accreted parautochthonous to allochtonous terranes, including the Yukon-Tanana, Slide Mountain, Quesnellia, and Stikinia terranes (Figure 1; Mortensen, 1992; Colpron et al., 2007a). The Yukon-Tanana terrane represents a mid-to-late Paleozoic continental arc that was rifted from the western margin of ancient North America (Laurentia) and resulted in the formation of the nearly coeval Slide Mountain back-arc basin during Late Devonian and Early to Middle Triassic time (Nelson et al., 2006). The geometric array of the Intermontane terranes exhibits an overall semiconcentric distribution of mainly magmatic-arc rocks, sedimentary successions, and oceanic rocks bordering western Laurentia between mid-Paleozoic to early Mesozoic times (Colpron et al., 2007a). Initiation of west-dipping subduction beneath the Yukon-Tanana terrane in the Permian led to arc magmatism, consumption of the Slide Mountain Ocean, and eventual collision of the Intermontane terranes with the modified North American margin in the Early Jurassic. The collision culminated in significant crustal shortening and thickening, followed by rapid unroofing and cooling over a broad region (Nelson et al., 2006; Beranek and Mortensen, 2011).

By the Early Cretaceous, the northern North American Cordillera was affected by highly heterogeneous deformation, which, from southwest to northeast that comprised (Figure 1; Nelson et al., 2013) (1) sinistral transpression along the southwestern margin (Coast belt); (2) dextral transpression in the Intermontane terranes; (3) east-vergent, ductile, and brittle deformation

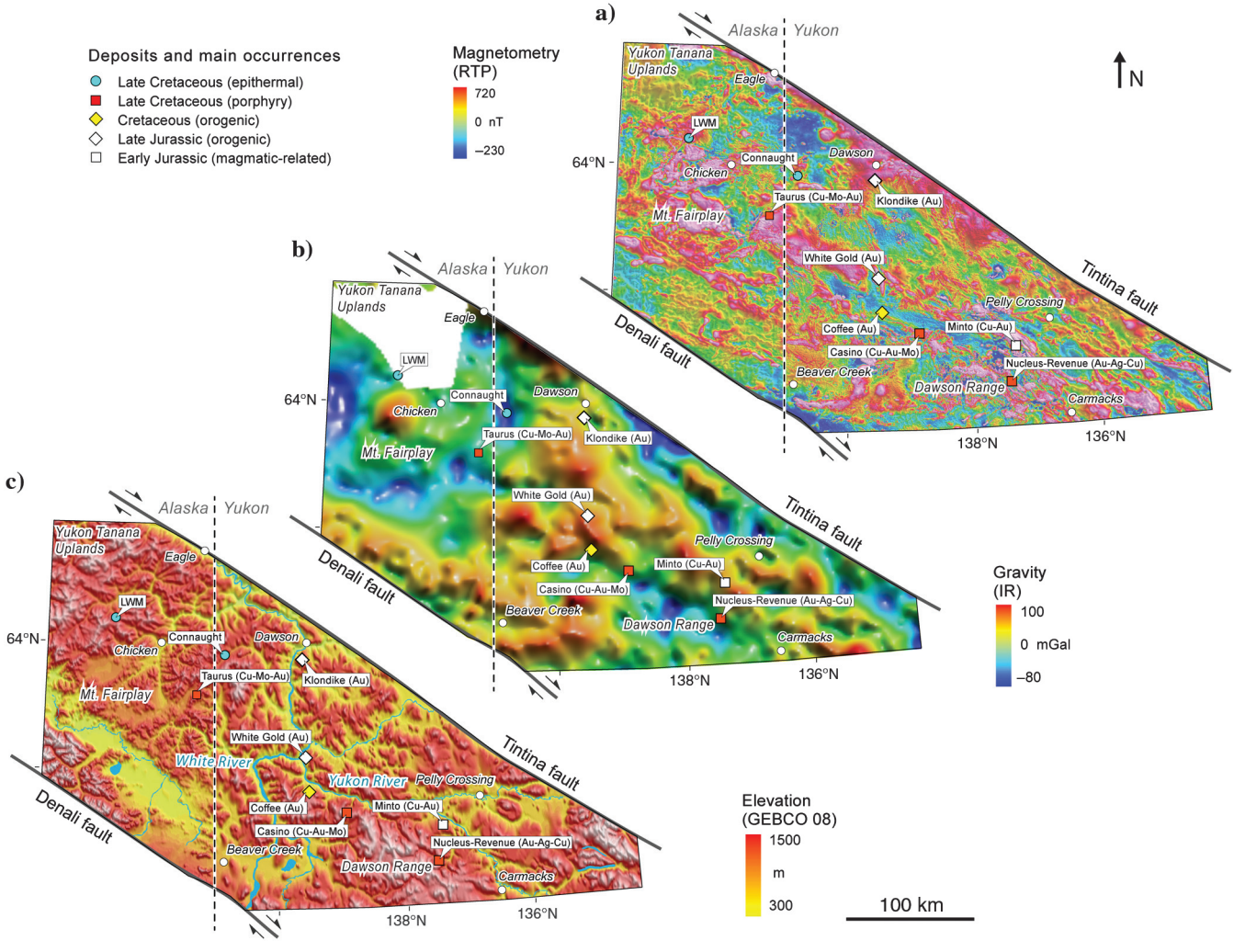

Figure 2. Geophysical grids from source data sets of the USGS, DGGS, and GSC (Buckingham and Core, 2012) and topographic data sets. (a) RTP magnetic grid, (b) isostatic residual (IR) gravimetric grid, and (c) GEBCO_08 DEM. Northeast-illuminated shaded grids.

along the eastern margin (Omineca belt and Rocky Mountain foreland fold and thrust belt); and (4) northwest-vergent ductile deformation, thrusting, and extension in the Selwyn basin and Yukon-Tanana Upland regions. By the mid-Cretaceous, tectonic extension dominated westernmost Yukon and eastern Alaska (Dusel-Bacon et al., 2002; Mair et al., 2006). In eastern Alaska, crustal extension was accommodated by footwall exhumation of Late Devonian to Early Mississippian orthogneiss of parauthochthonous North American affinity along low-angle normal faults, with Yukon-Tanana terrane comprising hanging wall units (Dusel-Bacon et al., 1995). At a similar time in British Columbia and southern Yukon, the northwest-trending Northern Rocky Mountain Trench (NRMT) developed as a major dextral strike-slip fault along the northern flank of the Intermontane terranes, which eventually propagated northwestward to form the nascent Tintina fault (Figure 1; Gabrielse, 1985). A series of subparallel dextral strike-slip faults (e.g., Teslin, Thibert, and Cassiar faults) splayed from the NRMT to the west–northwest into the Intermontane terranes (Gabrielse et al., 2006).

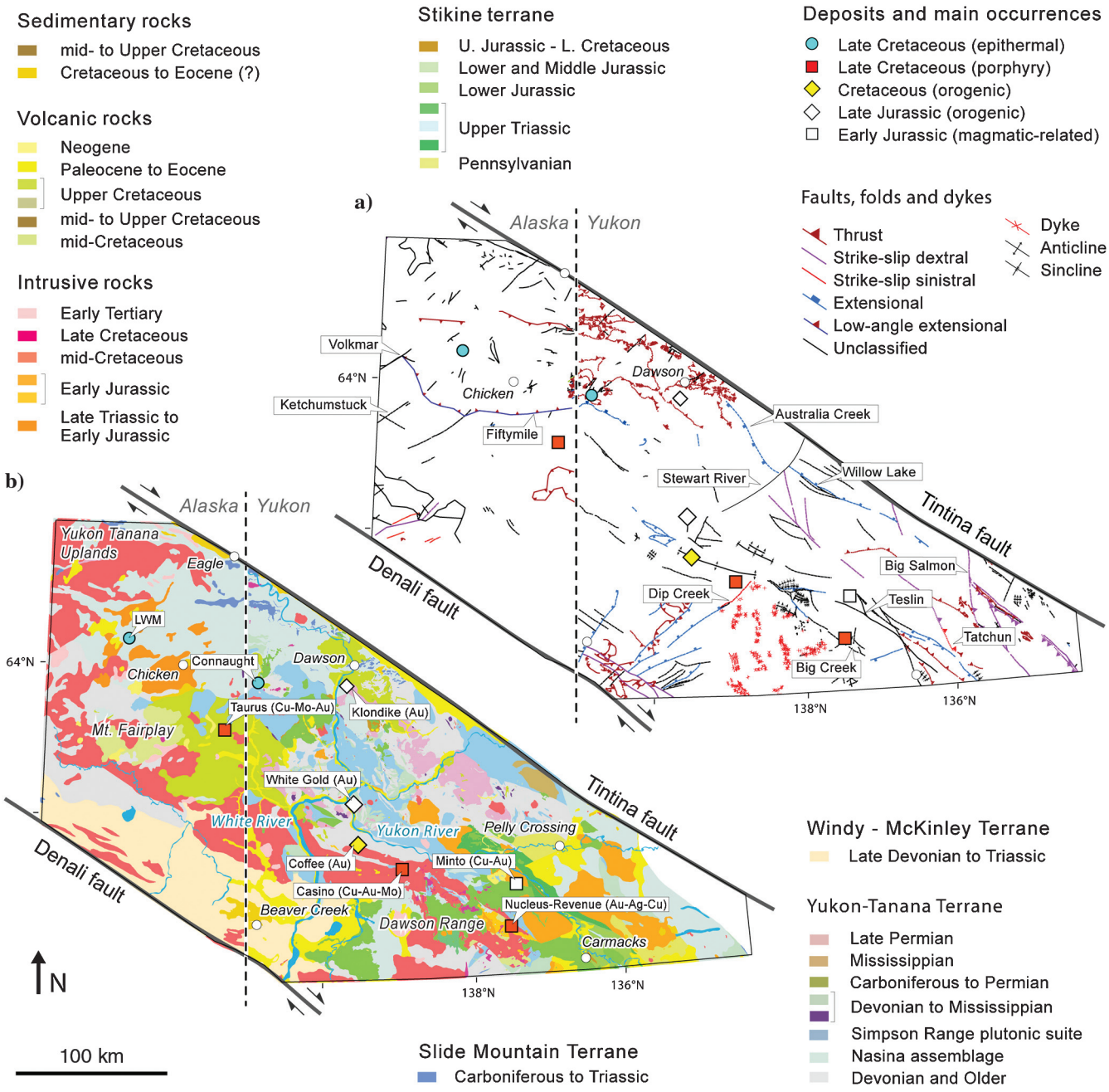

Figure 3. Geologic and structural data sets used for the current interpretation. (a) Compilation of known faults, folds, and dikes (e.g., Gabrielse, 1985; Mortensen, 1990; Dusel-Bacon et al., 2002; Gabrielse et al., 2006) and (b) geologic map compiled from several sources (Foster, 1976; Beikman et al., 1980; Gordey and Makepeace, 2001; Szumigala et al., 2002; Gordey and Ryan, 2005; Colpron et al., 2007b; Garrity and Soller, 2009; Ryan et al., 2010, 2013; Staples et al., 2013).

During the mid- to Late Cretaceous, the Big Creek fault propagated northwest from the Teslin fault along the northeastern flank of the Yukon's Dawson Range (Figure 3; Tempelman-Kluit, 1984; Johnston, 1999). Late Cretaceous to early Cenozoic east–northeast- to northeast-oriented dextral strike-slip faults (e.g., Kaltag, Iditarod-Nixon Fork, Farewell-Denali, Castle Mountain, Bruin Bay, and Border Ranges faults) occurred along the western limb of the southern Alaska orocline (Figure 1; Glen, 2004). In southwestern Alaska, at least four periods (~100, ~70, ~60, and ~30 Ma) of sedimentation, folding, magmatism, and mineralization occurred alongside an accumulated dextral displacement between ~134 and ~90 km on the Farewell-Denali fault and Iditarod-Nixon Fork faults, respectively (Figure 1; Miller et al., 2002).

Postaccretionary plutonic suites, resulting from Cretaceous to Paleogene subduction outboard of the Intermontane terranes affected a broad area of the northern Cordillera (Figure 1; Gabrielse et al., 2006; Mair et al., 2006). Early to mid-Cretaceous magmatism was widespread throughout Alaska and Yukon, with highly oxidized plutonic suites distributed as northwest–southeast-oriented arcs parallel to the orogen (Figure 3; Hart et al., 2004a; Mair et al., 2006). In the study area, these include I-type plutons of the ca. 110–103 Ma Whitehorse plutonic suite, known locally as the *Dawson Range batholith*. Coeval-reduced plutons occur throughout the back-arc (Figure 3; Mortensen et al., 2000; Baker and Lang, 2001; Hart et al., 2004b).

The accumulated northwestward translation of the Intermontane terranes by northwest-trending dextral strike-slip faults since the Cretaceous is geologically constrained to be ~860 km (Gabrielse et al., 2006). Restoration of magnetic domains across the northwest-trending Tintina fault indicates that this fault accommodated about 490 km of the total translation in the Eocene (Saltus, 2007). Near the bend of the Alaskan

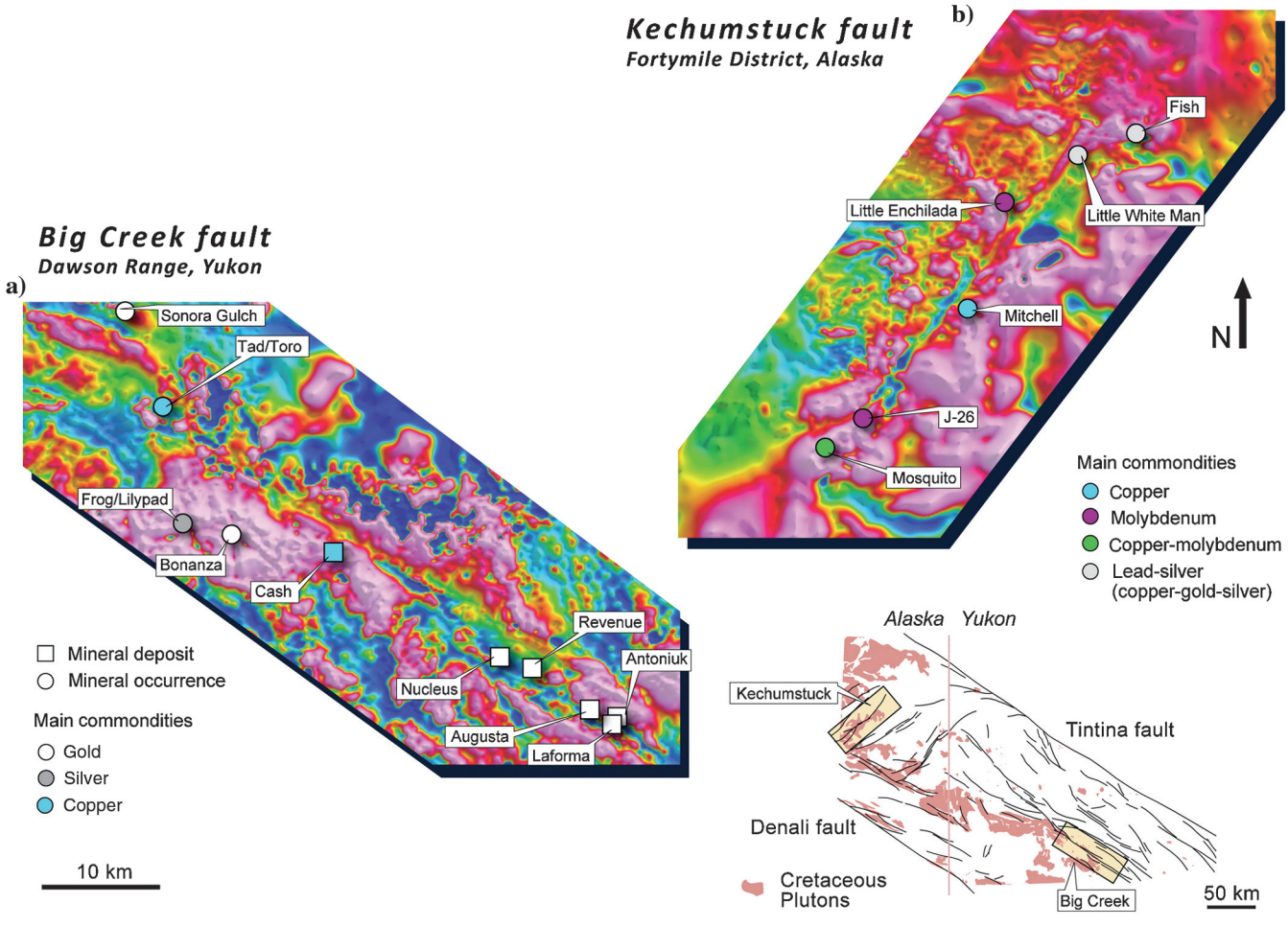

Figure 4. Two examples of northwest- and northeast-oriented high-frequency magnetite-destructive faults of the RTP data set of western Yukon and eastern Alaska. Both fault systems host a series of Cretaceous magmatic-related mineral occurrences and deposits. (a) The Big Creek fault shows a ~150-km-long, magnetite-destructive signal and a topographic trench. This fault bounds the Dawson Range to the northeast and limits the spatial distribution of Cretaceous plutons. (b) The Kechumstuk fault mainly places Cretaceous intrusive rocks to the southeast in contact with Devonian and older metamorphic rocks to the northwest along a ~100-km-long, magnetite-destructive discontinuity. A magnetite-additive signal is observed along its northeastern fault trace. Both magnetite-destructive faults divide domains of contrasting magnetic intensity and texture.

orocline, and between the Denali and Tintina fault systems of eastern Alaska, seismic moment tensor solutions reveal that a series of active north–northeast-trending sinistral strike-slip faults may accommodate clockwise block rotations in response to north-oriented compression (Page et al., 1995).

The structural interpretation of aeromagnetic lineaments in this contribution is naturally biased toward Cretaceous and younger strike-slip and transtensional fault systems because these structures are most clearly expressed as aeromagnetic and geologic discontinuities. Lower-angle fold-and-thrust features recognized in the aeromagnetic data or recorded on geologic maps are not generally included in the structural interpretation; these comprise the background structural architecture of the region and do not play an important role in magmatic-hydrothermal mineralization in the region. However, the overprinting of orogen-parallel strike-slip faults on the preexisting fold-and-thrust architecture of the Intermontane terranes makes differentiating these two structural styles locally ambiguous.

Fault- and nonfault-related aeromagnetic lineaments

The magnetic expression of a fault depends not only on the inherited magnetic susceptibility of the rocks involved, but also on the geologic processes that affect the rocks' magnetic properties during and after fault development (Lapointe et al., 1984; Clark, 1997). Deformation, metamorphism, magmatism, hydrothermal alteration, and weathering may result in changes in grain size, crystallization environment, silica saturation, metamorphic degree, and oxidation state (Grant, 1985; Lapointe et al., 1986; Latham et al., 1989; Isles and Rankin, 2013). Addition of magnetic minerals within a fault or fracture can result from emplacement of mafic magma along the structure. It may also be a consequence of metasomatic or hydrothermal alteration with introduction of magnetic minerals, such as magnetite in some iron oxide-copper-gold and skarn systems (Gunn and Dentith, 1997; Direen and Lyons, 2007). Destruction of magnetic minerals within a structure by metasomatism and hydrothermal alteration, or by oxidative weathering, results in a decrease in magnetic susceptibility (and/or magnetic remanence) due to conversion of magnetic ferrous minerals to ferric oxides or oxyhydroxides (Airo, 2002; Airo and Mertanen, 2008; Isles and Rankin, 2013). For instance, quartz deposition in low-sulphidation epithermal vein systems hosted by tensional fractures in homogeneous unaltered andesitic-basaltic units will result in high-frequency magnetite-destructive lineaments (Allis, 1990; Irvine and Smith, 1990). A decrease in magnetic susceptibility may further result from grain-size reduction in a sheared brittle fault (e.g., fault gouge; Wintsch et al., 1995; Maidment et al., 2000), or due to dynamic recrystallization under plastic deformation (e.g., mylonite fault rocks; Goldstein, 1980; Henderson and Broome, 1990).

Aeromagnetic lineaments with geologic significance are as follows: (1) magnetite-destructive discontinuities (e.g., strongly weathered fault contact), (2) highly magnetic discontinuities (e.g., ophiolite along a fault contact), (3) lineaments of contrasting magnetic response relative to country rocks (e.g., felsic or mafic dike), (4) aeromagnetic-anomaly edges (e.g., plan-view-elongated intrusive contact), (5) subparallel lineaments arising from, e.g., schistosity or sedimentary layering, or (6) a single minor lineament placing sets of minor, subparallel lineaments in contact (e.g., angular unconformity). Aeromagnetic lineaments may also arise from human features such as fences, pipes, power transmission lines, etc. Additional artifacts also commonly result from nonuniform survey flight clearance to ground or due to incorrect or nonexistent topographic corrections (Luyendyk, 1997).

In this contribution, the term "magnetite-destructive lineament" corresponds to a linear or curvilinear, high-frequency aeromagnetic feature of lower intensity than the surrounding region. In contrast, a "magnetite-additive lineament" has high frequency and higher intensity than the surrounding region. A lineament is a "discontinuity" where it defines the boundary between adjacent domains of differing magnetic character (i.e., frequency, amplitude, intensity, and magnetic fabric orientation). Because magnetic domains correlate with rock packages with distinct lithologic and petrophysical properties, discontinuities of either magnetite-destructive or magnetite-additive type are reasonably interpreted as geologic faults. Magnetite-destructive discontinuities (i.e., lineaments that mark a magnetic domain change) are interpreted as faulted lithological contacts in which magnetite has been removed by fluid interaction. Conversely, magnetite-additive discontinuities are interpreted as faulted lithological contacts along which a mafic dike has intruded, or along which magnetite has precipitated from hydrothermal fluid. Where a magnetite-destructive lineament does not coincide with a magnetic domain boundary, it is reasonably interpreted as a fracture or as a dike of lower magnetic susceptibility than its host rocks. Similarly, a magnetite-additive lineament within a single magnetic domain is most reasonably interpreted as a mafic dike. Obviously, a geologic structure without an anomalous magnetic signature is invisible if it juxtaposes domains with the same magnetic expression.

Data sets

The approach to structural interpretation in this study uses four main layers (Figures 2, 3, and 5): (1) a RTP aeromagnetic grid (Figure 2a) and derivatives (analytic signal, horizontal gradient, tilt angle filter, upward-continued residuals, residual pseudogravity, first vertical derivative (1VD), Figure 5a and 5b); (2) an IR gravimetric grid (Figure 2b) and derivatives (residuals and 1VD grids, Figure 5c); (3) DEMs of various types and resolutions (Figure 2c); and (4) geologic maps and structural data compiled at 1: 400,000 scale (Figure 3).

Mineral deposit names and locations were primarily taken from Yukon Geological Survey MINFILE (Yukon MINFILE, 2010) and Alaska Resource Data File (ARDF) (Grybeck, 2008) databases and updated with current literature on deposit age and style (Allan et al., 2013).

The aeromagnetic data used in this study were obtained from regional government compilations in Alaska (Connard et al., 1999; DGGS et al., 1999; Saltus, 2007; Burns et al., 2008, 2011) and Yukon (Hayward et al., 2011; Geological Survey of Canada, 2012). Both fixed-wing and helicopter surveys are represented in the source data, and flight line spacing varied from approximately 400 m over most of the study area to 1200 m. Magnetic data were reprojected, gridded, continued (to a higher or lower elevation), reduced to the pole (by transforming bipolar magnetic anomalies to monopolar anomalies centered over their magnetic source for a more accurate representation; Baranov and Naudy, 1964), and merged as appropriate (by A. Buckingham and D. Core, Fathom Geophysics LLC). Aeromagnetic data were not terrain-corrected. The resulting seamless RTP grid was constructed with a 100-m cell size and an equivalent 100-m terrain clearance. This and all other geophysical grids were color-stretched and directionally shaded (Figure 2a). The RTP magnetic grid is the foundation of the lineament interpretation in this study (Figure 5).

The gravity data set used in this study is an IR gravity grid with a 2-km cell size (Figure 2b; produced by A. Buckingham and D. Core, Fathom Geophysics LLC). Source data in Yukon have an average grid spacing of 10 km (Canadian Geodetic Information System, 2012), whereas gravity stations in eastern Alaska (Morin, 2007; Saltus et al., 2008) are sporadically spaced and locally sparse, resulting in a significant data coverage gap in the northwestern quadrant of the grid (Figure 2b). The IR gravity grid provides a representation of the density distributions within the upper crust as it subtracts long-wavelength anomalies of deep crustal or mantle sources from Bouger anomalies (Heiskanen and Moritz, 1967; Simpson et al., 1986). Lineaments interpreted from the RTP magnetic data set were evaluated against three upward-continued residuals IR gravity grids (20–10 km, 10–5 km, and 5–1 km) as well as against the 1VD of the IR gravity grid.

DEMs were used for geomorphologic interpretation of geologic structures in this study. Data include the regional GEBCO_08 DEM (IOC et al., 2003) and the ~30-m resolution ASTER GDEM2 data set (Figure 2c; METI and NASA, 2011). The ASTER GDEM2 data were appropriate for regional-scale interpretations, although this DEM is still under preliminary development and includes local "pit" and "mole run" artifacts that arise from boundary stacking (Arefi and Reinartz, 2011; Tachikawa et al., 2011).

Geologic information for the study area was compiled from various government sources (Foster, 1976; Beikman, 1980; Foster et al., 1994; Gordey and Make-

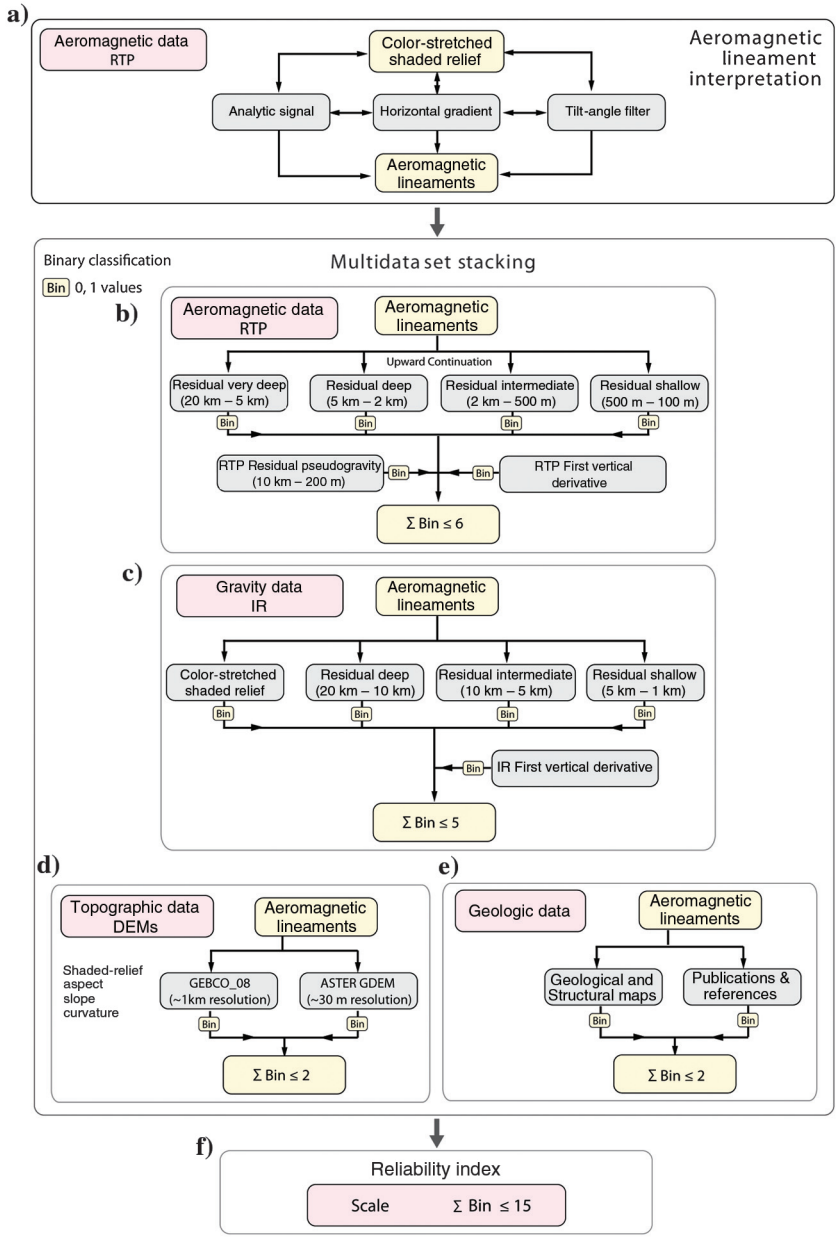

Figure 5. Workflow used for aeromagnetic lineament interpretation and data-stacking methodology for assessment of lineaments as faults. The methodology integrates geophysical, topographic, and geologic data sets for the generation of a lineament reliability index.

peace, 2001; Szumigala et al., 2002; Gordey and Ryan, 2005; Colpron et al., 2007b; Garrity and Soller, 2009; Murphy, 2009; Ryan et al., 2010, 2013). These maps provided various degrees of structural information, but for the most part are structurally underinterpreted as a consequence of poor rock exposure. A series of additional published maps (e.g., Gabrielse, 1985; Mortensen, 1990; Dusel-Bacon et al., 2002; Gabrielse et al., 2006; Staples et al., 2013) were georeferenced and incorporated into the structural interpretation.

Interpretation of the geophysical data sets was carried out at 1: 400,000 scale within a geographic information system platform (ArcGIS 10.1) using the North American Datum 1983 (NAD 83) Universal Transverse Mercator (UTM) Zone 7N projected coordinate system.

Aeromagnetic lineament interpretation

The structural interpretation in this study is based on a systematic, multidata set "stacking" methodology, in which lineaments are compared against various data layers to provide a measure of geologic confidence in the feature (Figure 5). The initial step in this procedure is the iterative extraction of lineaments from aeromagnetic grids (Figure 5a). This was achieved by manually tracing lineaments on a series of color-stretched and shaded-relief RTP aeromagnetic maps. The use of the analytic signal, horizontal gradient, and tilt angle filter grids in combination helped reduce human bias, detect artifacts, and refine lineament traces. The methodology did not employ any automatized structure detection algorithms.

The use of aeromagnetic data as the starting point for structural interpretation is warranted in this study, not only because the aeromagnetic data have continuous coverage at a resolution appropriate for exploration targeting, but also because the data contain projected 3D information on exposed and buried geologic units and structural features (Figure 2a). The aeromagnetic grids benefit geologic interpretations by providing additional information on metamorphic and sedimentary fabrics, as well as intrusive and stratigraphic contacts.

The aeromagnetic lineament interpretation was performed on a RTP grid that was not terrain-corrected and may be susceptible to magnetic gradients arising from nonuniform flight clearance over steep topography (Figure 2c). Although false aeromagnetic lineaments could arise along topographic trenches or ridges as a consequence of terrain-induced effects (Luyendyk, 1997), this problem may also be present in draped magnetic data (Grauch and Campbell, 1984). For this reason, we emphasize that magnetite-destructive or magnetite-additive lineaments that overlap topographic trenches or ridges correlate with real geologic faults when juxtapose contrasting aeromagnetic domains.

Aeromagnetic, gravity, and topographic filters

Grids of aeromagnetic and gravity residuals were used as inputs for the structural interpretation of this study (Figure 5b and 5c). Spectral information was not used for the definition of residual levels, due to the significant uncertainties in using this approach for depth estimate calculations (Spector and Grant, 1970, 1975; Spector, 1985). As recommended by Gunn (1997), geologic constraints such as the thickness of volcanic-sedimentary piles, depth to basement, regolith thickness, and other geologic observations were used to define depth slices for residual levels.

To represent depth surfaces in potential field data, upward-continued data sets were produced following a similar methodology to Jacobsen (1987), whereby a band-pass filter is used to separate causative sources at various depths. Jacobsen (1987) considers that the observed magnetic or gravity field is the result of the sum of the regional field, the residual field, and aggregate noise. To isolate a regional field at a given depth (z0), the observed field was upward-continued to a height above the land surface equivalent to twice its depth (2*z0). Therefore, to estimate the magnetic or gravity response from an equivalent source at a depth range between z1 and z2, we obtain the difference between upward continuations at heights 2*z2 and 2*z1.

Magnetic filters

Geologic considerations for the selection of the four upward-continuation levels applied to the aeromagnetic data are described below:

1) All upward-continuation levels approximate crustal depths less than ~10 km. At a typical geothermal gradient (e.g., 30°C/km), rocks at this depth are expected to be well below the Curie temperature of magnetite (585°C) and have the potential to generate a magnetic response.
2) 20–5 km (equivalent to a ~10–2.5 km-depth slice): Depth range for intermediate to deep brittle crustal conditions. Across the Canadian Cordillera, regional crustal refraction profiles provide a framework of crustal thickness and regional seismic velocity variations. These consistently indicate that P-wave velocities only increase at depths higher than ~25 km (Cook et al., 2004). For this depth range, brittle conditions occur when considering an average geothermal gradient of 30°C/km in crust of average composition (Dragoni, 1993). Due to its very long wavelength, this residual range is only sensitive to large-wavelength aeromagnetic lineament systems that may result from significant downdip extents (Figure 6c).
3) 5–2 km (equivalent to a ~2.5–1 km-depth slice): Depth range for shallow upper crust with metamorphic assemblages and Mesozoic plutons that occur below unmetamorphosed volcanic and sedimentary rocks. This depth range shows greater lineament density useful for the recognition of shorter secondary aeromagnetic lineaments. At this range, the recognition of major lineament systems is still plausible (Figure 6d).

4) 2 km–500 m (equivalent to a ~1 km–250 m-depth slice): Depth range appropriate for unmetamorphosed Mesozoic and Cenozoic volcanic and sedimentary rocks (e.g., Upper Cretaceous volcanic rocks and mid- to Upper Cretaceous sediments (Figure 1). This residual range provides valuable information on secondary and tertiary faults linked to large-scale fault systems and therefore contributes key information on the interpretation of structural styles and kinematics (Figure 6e).
5) 500–100 m (equivalent to an ~250–50 m-depth slice): Depth range appropriate for regolith and surficial deposits. The large number of short-wavelength artifacts present in this residual range results in greater structural uncertainty (Figure 6f).

In addition to the RTP residuals, a 1VD RTP grid was used to highlight high-frequency signals derived from shallow magnetic sources (Milligan and Gunn, 1997; Figure 5b). Finally, a pseudogravity-transformed RTP grid was upward-continued between 10 km and 200 m for residual calculations (Figures 5b and 6b). The pseudogravity transformation implies an approximate conversion of magnetic to gravity data by changing its rate of decay from the inverse cube of the distance to source to the inverse square of the distance to source. This transformation enhances the anomalies associated with deep magnetic sources at the expense of shallow sources (Hildenbrand, 1983).

Gravity filters

For the IR gravity grid, we calculated upward-continued residuals for ranges 20–10 km, 10–5 km, and 5–1 km representing sources shallower than ~10-km depth (Figure 5c). The first two residual levels aim for longer wavelength signals representing regional deeper sources. On the contrary, the 5–1 km upward-continued residual (equivalent to a ~2.5 km–500 m-depth slice) provides information of shallower sources located below the approximate regolith and surficial deposits level. Finally, a 1VD filter was used to highlight high-frequency and short-wavelength gravity signals.

Topographic filters

Two DEM grids were used in combination with few topographic filters to determine the geomorphologic expression of lineaments interpreted from the RTP grids (Figure 5d). Topographic filters were computed from the regional GEBCO_08 (IOC et al., 2003) and higher resolution ASTER GDEM2 (METI and NASA, 2011) data set using the topographic analysis tools in ArcGIS 10.1 software (ESRI, 2013). Separate topographic filters were applied to highlight slope aspect, slope steepness, and slope curvature. The hill-shaded relief grid is generated from a raster by considering the illumination angle and shadows. The slope grid identifies the rate of maximum change in the z-value from each cell. The aspect grid generates a map for slope direction and it identifies the downslope direction from the maximum rate of elevation change. The curvature grid considers the second derivative of the slope, i.e., its concavity or convexity. Finally, drainage divides and river systems were extracted from the ASTER GDEM2 data using ArcGIS hydrology tools (ESRI, 2013) and were interpreted for neotectonic

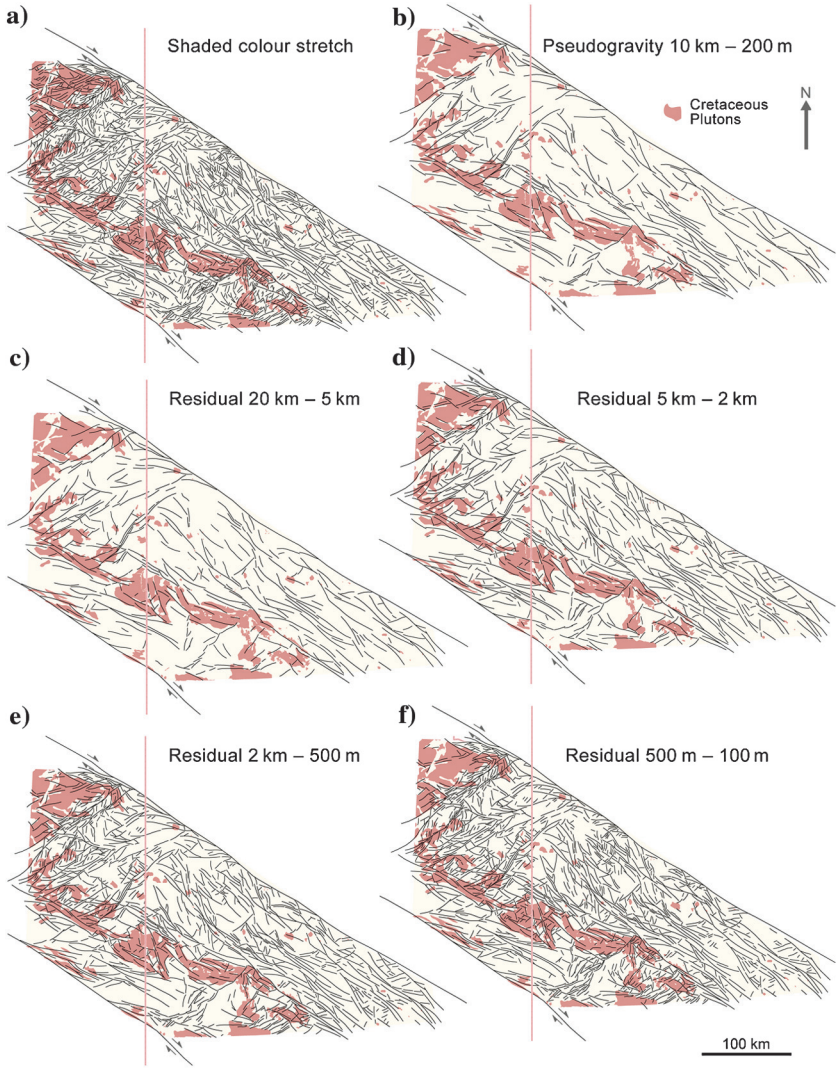

Figure 6. Aeromagnetic lineaments evaluated across a series of upward-continued residual filters of the RTP grid. (a) Unfiltered color stretch, (b) pseudogravity RTP (10 km–200 m), (c) residual very deep (20–5 km), (d) residual deep (5–2 km), (e) residual intermediate (2 km–500 m), and (f) residual shallow (500–100 m).

geomorphologic features (e.g., sag ponds, beheaded streams, river offsets, etc.).

Multidata set stacking methodology

The approach to structural interpretation in this study is based on the premise that geologic faults should be expressed in multiple types of geospatial information. Therefore, a stacking procedure was developed that compares lineaments initially interpreted from the aeromagnetic data (see above) against gravimetric, topographic, and geologic data layers (Figure 5). At the 1: 400,000 scale of interpretation, each aeromagnetic lineament is visually queried against the RTP-derivative grids (residuals, 1VD, and pseudogravity), IR gravity grids, digital topography, and regional geologic maps. The lineament is assigned a value of one for each data layer in which it is expressed, or a value of zero in which the feature is absent. Depending on a lineament's expression in each data set, these equally weighted scores give a sum in the range of zero to 15, referred to herein as the "reliability index" (Figure 5f). Although each data input is equally weighted, the effective weighting of different data types depends on the number of input grids for each (i.e., six for magnetic data, five for gravity data, two for topographic data, and two for geologic data).

Following the integration of aeromagnetic and gravity data inputs (Figure 5b and 5c), the aeromagnetic lineaments were compared against similar-trending topographic trenches and ridges of the DEMs (Figure 5d). For this purpose, lineaments were compared with shaded relief, aspect, slope, and curvature models. The study area is located at high latitudes (north of ~61°N), which results in higher sun exposure on south-facing permafrost slopes. This results in steeper north-facing slopes, limiting our capability to correctly interpret fault scarps and fault blocks tilting. Finally, aeromagnetic lineaments were compared against known faults, dikes, and geologic contacts on published geologic maps (Figures 3 and 5e). Although this methodology weighs all data sets equally, widely accepted faults on published geologic maps most commonly have a strong topographic and geophysical expression, resulting in a higher reliability index.

The sum of the binary values assigned to individual aeromagnetic lineaments yields a reliability index, which represents the level of confidence in the lineament as a geologic structure (Figures 5f and 7). The digital database allows the interpreter to query for any

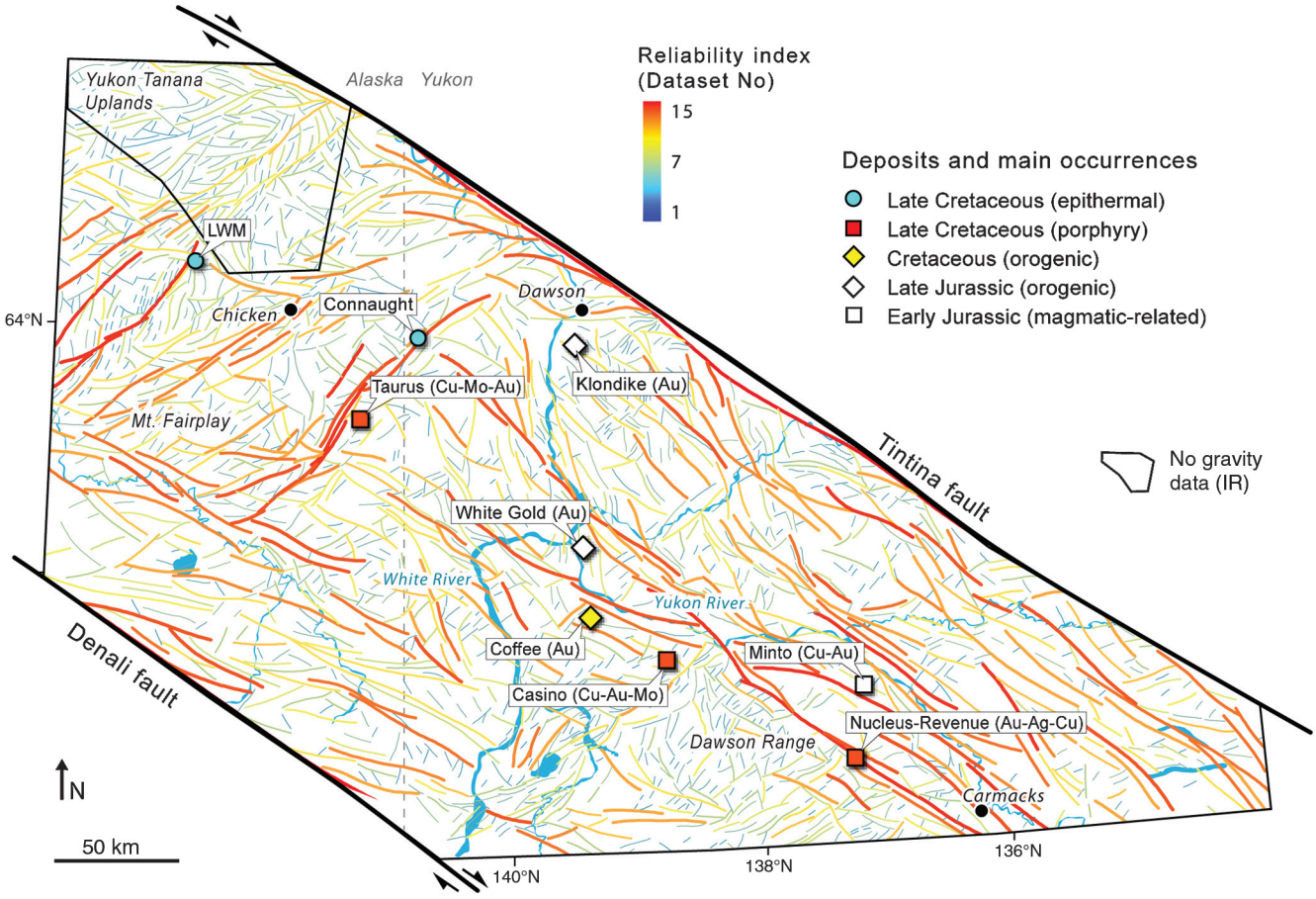

Figure 7. Reliability index map based on multidata set-stacking methodology.

input associated with an aeromagnetic lineament. The database can also be used to test and predict the effectiveness of a stand-alone aeromagnetic, gravity, or geomorphologic interpretation of a structure.

Lineament system map

A key objective of the aeromagnetic interpretation is the generation of a lineament system map as an approach to mapping fault systems (e.g., McClay and Bonora, 2001). This is constructed by evaluating the results of all components of the stacking methodology and by carrying out spatial analysis of aeromagnetic lineaments (Figure 8). The spatial distribution and geometric characteristics of aeromagnetic lineaments were analyzed by querying their length, azimuthal, and spatial density. Spatial density analysis was especially useful for the grouping of individual aeromagnetic discontinuities and lineaments into lineament systems (Figure 9).

The lineament system map was constructed based on: (1) calculation of a normalized length scale for the entire population of aeromagnetic lineaments, (2) azimuthal analysis using line-azimuthal and length-weighted rose diagrams, resulting in two predominant structural orientations (west–northwest- to north–northwest-trending and north–northeast- to east–northeast-trending; Figures 8a and 9a), (3) data-stack sorting based on a histogram of reliability index values (Figure 8b) with the top three of five groups assigned geographic names after existing geologic faults, rivers, or geographic locations, and (4) spatial density analysis of aeromagnetic lineaments for the recognition of high-density structural zones or corridors (Figure 9b). Line density analysis was performed using the ArcGIS 10.1 Spatial Analyst module, using unweighted and length-weighted approaches (ESRI, 2013). A third line density calculation was weighted according to the reliability index of each lineament (Figure 9b). Individual aeromagnetic discontinuities and lineaments were

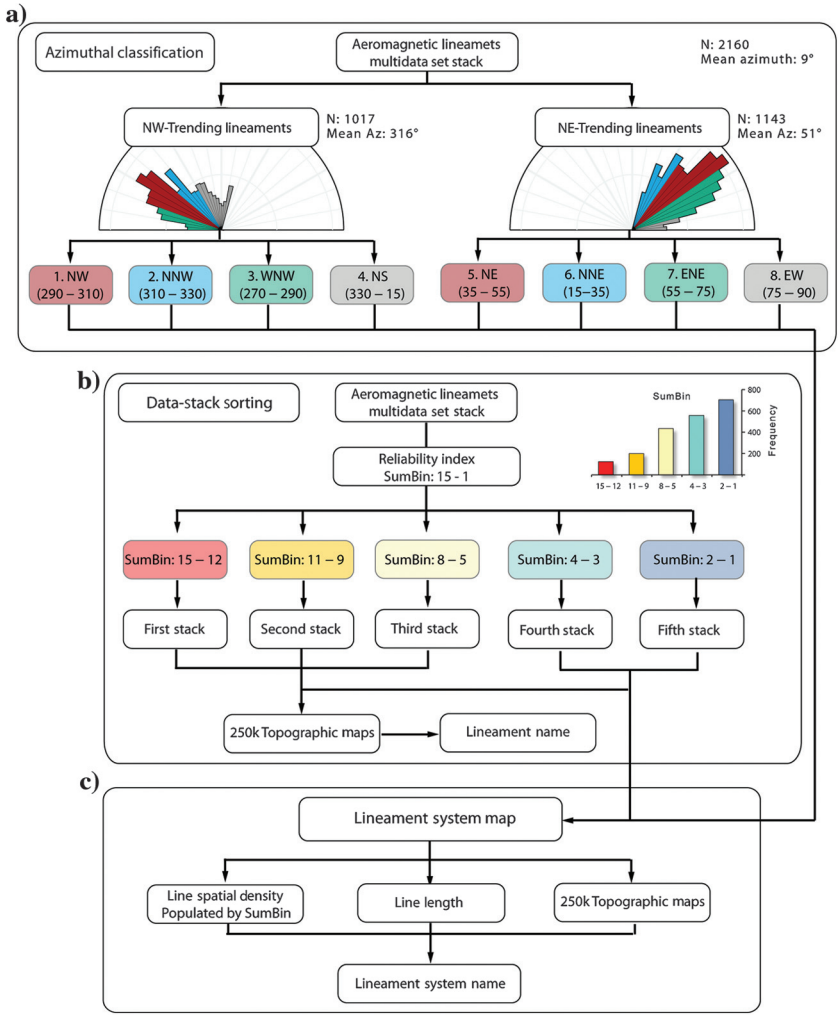

Figure 8. Structural classification workflow for spatial organization of aeromagnetic lineaments. (a) Spatial classification using lineament orientations, (b) data-stack classes using binary attributes, and (c) spatial and geographic classification for fault systems.

grouped into density corridors of coherent spatial and geometric characteristics.

Azimuthal classification

Following a series of mechanical and geometric assumptions, we infer that a number of interpreted aeromagnetic lineaments and discontinuities correspond to steep-dipping fracture and faults arrays. This is particularly applicable to magnetite-destructive or magnetite-additive discontinuities that correlate with aeromagnetic domain changes and that have high reliability index scores (Figures 4 and 5).

Riedel shear strike-slip fault geometries

Aeromagnetic lineaments define semiorthogonal northwest- and northeast-trending arrays (Figures 8a and 10). To interpret the geometries and investigate the kinematics associated with individual aeromagnetic lineaments, a Riedel shear strike-slip fault system model is applied (Tchalenko, 1970; Sylvester, 1988). The use of this model is justified by the presence of continental-scale northwest-trending dextral strike-slip faults (e.g., the Tintina — NRMT and Denali faults) and by the development of a series of major and subparallel synthetic faults (e.g., Teslin, Thibert Cassiar and Big Creek faults; Tempelman-Kluit, 1984; Johnston, 1999; Gabrielse et al., 2006). We also used the Riedel shear model for east–northeast- to northeast-oriented fault systems based on previously recognized sinistral strike-slip faults in eastern Alaska (e.g., Shaw Creek, Volkmar, Kechumstuck, and Sixtymile-Pika faults; Foster, 1976; Hansen and Dusel-Bacon, 1998; Dusel-Bacon et al., 2002, 2006; Allan et al., 2013; Day et al., 2014) and

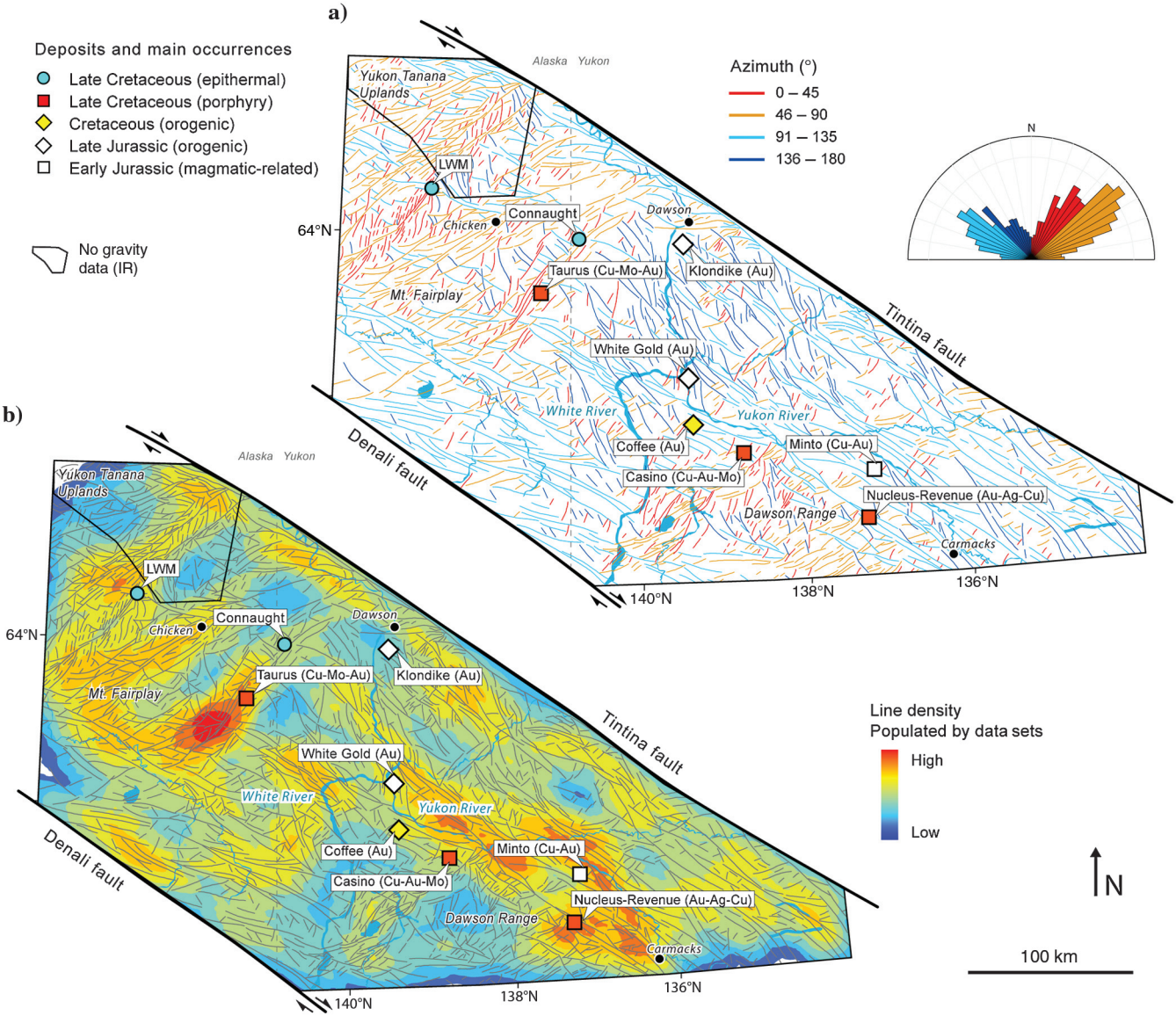

Figure 9. Aeromagnetic lineament length and density maps. (a) Line azimuthal map showing color codes every 45°, (b) line spatial density grid populated by summation of all values of the stacking methodology for multidata set lineament confidence classification. First to fourth data-stack groups of aeromagnetic lineaments overlain on density grid.

shear zones (Black Mountain tectonic zone; O'Neill et al., 2010).

Interval classes 1 and 5 include aeromagnetic lineaments considered subparallel (±10°) to the two main shear zones of N60°W and N45°E orientation (Figure 10). For individual azimuthal groups, two additional orientations classes (classes 2 and 3 for northwest-trending lineaments and classes 6 and 7 for northeast-trending lineaments) are subdivided according to R and P synthetic Riedel shears. These trend within 15° ($\theta/4$ assuming a θ angle of 60°) to the azimuthal limits of the two main N60°W and N45°E shear zones. Deviation errors of ±5° have been arbitrary added to the outer limit of P and R Riedel shears intervals. Two additional azimuthal classes (classes 4 and 8), which include R′ antithetic Riedel shears orientations, were defined for each main shear zones. Class 4 corresponds to lineaments oriented between the limits of class 2 (N30°W strike) and class 6 (N15°E strike) R Riedel shears. East–northeast-trending class 8 corresponds to lineaments oriented between the limits of class 7 (N75°E strike) and class 3 (N90°E strike) P Riedel shears. We interpret these two additional and highly oblique orientations classes as structures accommodating antithetic strike-slip and/or oblique extension.

Interpretation of lineament orientations according to the Riedel shear strike-slip fault model suggests that northwest-trending fault systems are predominantly dextral and that northeast-trending shear zones are predominantly sinistral, each with associated P and R synthetic Riedel shear structural elements (Figure 10).

Structural interpretation

A structural interpretation of the lineament systems and aeromagnetic discontinuities was carried out within the postaccretionary tectonic and structural framework of the western Alaska and eastern Yukon Cordillera. An obvious outcome is that northwest-trending aeromagnetic lineaments and faults are prominent east of the Alaska-Yukon border, whereas the Alaskan portion is dominated by northeast-trending structures (Figure 10). This transition in structural style corresponds spatially with a major northeast-trending gravity low that crosses the Yukon-Alaska border between the towns of Dawson, Yukon and Chicken, Alaska (Figure 2). Transecting this gravity low is the northeast-trending Sixtymile-Pika fault, which exhibits sinistral offset of several geologic markers (Allan et al., 2013).

Northwest-trending aeromagnetic features correspond to major geologic contacts and the Cretaceous Dawson Range magmatic arc (Gordey and Makepeace, 2001; Hart et al., 2004a), as well as to previously recognized orogen-parallel fault systems in western Yukon (Figures 1 and 3; e.g., Tintina, Denali, Big Creek, Teslin, and Tatchun faults; Tempelman-Kluit, 1984; Johnston, 1999; Gabrielse et al., 2006; Colpron et al., 2007b; White et al., 2012). Northeast-trending aeromagnetic features correlate to major geologic contacts and Cretaceous plutons in eastern Alaska (Figure 3; Foster, 1976; Moll-Staccup, 1994; Szumigala et al., 2002). These also correlate closely to previously recognized northeast-trending faults in eastern Alaska (Figures 1 and 3) (e.g., Shaw Creek, Volkmar, Kechumstuck, and Sixtymile-Pika faults; Foster, 1976; Hansen and Dusel-Bacon, 1998; Dusel-Bacon et al., 2002; Dusel-Bacon et al., 2006; Allan et al., 2013; Day et al., 2014), shear zones (Black Mountain tectonic zone; O'Neill et al., 2010) and radiometric lineaments (Wilson et al., 1985). Transecting the Dawson Range of western Yukon, the Dip Creek fault is the most prominent orogen-perpendicular structure (Figure 11; Templeman-Kluit, 1974; Johnston, 1999; Ryan et al., 2013). Northeast-trending faults also result in abrupt offsets and width variations in the mapped exposure of northwest-trending Cretaceous plutons in the study area (Sánchez et al., 2013). Both northeast- and northwest-trending faults of eastern Alaska and western Yukon commonly result in linear geomorphologic trenches and lateral offsets of river systems.

Northwest-trending fault systems

Ten major northwest-trending aeromagnetic lineaments and discontinuities representing steep-dipping fault systems are recognized in the study area. These are oriented subparallel to the regional Cordilleran deformation fabric, mid-Cretaceous Dawson Range magmatic arc, and Tintina and Denali faults (Figure 11). These northwest-trending structural systems may constitute fault branches and splays that link to regional-scale dextral strike-slip systems such as the NRMT, Teslin fault, and nascent Denali and Tintina faults (Figure 1). Examples of previously known northwest-trending faults with high-frequency and low-amplitude magnetic response include the Teslin, Big Creek, and Tatchun faults (Figure 11; Gordey and Makepeace, 2001; Gabrielse et al., 2006; Colpron et al., 2007a; White et al., 2012).

Two apparently significant structural corridors are the Dawson Range–Tanacross North and Mount Tyrrel–Oglive fault systems (Figure 11). These are represented by highly continuous and linear magnetic patterns that continue northwestward from the Big Creek and Teslin faults, respectively (Figure 11). These regional magnetic discontinuities have strike lengths of ~300 km, extending from the southeastern edge of the grid almost as far as the Yukon-Alaska border. These and other major northwest-trending fault systems are characterized by north–northwest to north-trending fault splays at their northwestern most tips (Figure 10a). These fault-tip splays are inferred to act as oblique extensional structures that accommodated subsidence at the termination of major dextral stike-slip faults. Local bends and structural linkages along strike of major fault traces are also observed along major northwest-trending fault systems (Figure 11). Along the Big Creek fault in the vicinity of Nucleus and Revenue gold deposits (Northern Freegold, 2012a, 2012b), an observed fault relay is interpreted to result in a local zone of transten-

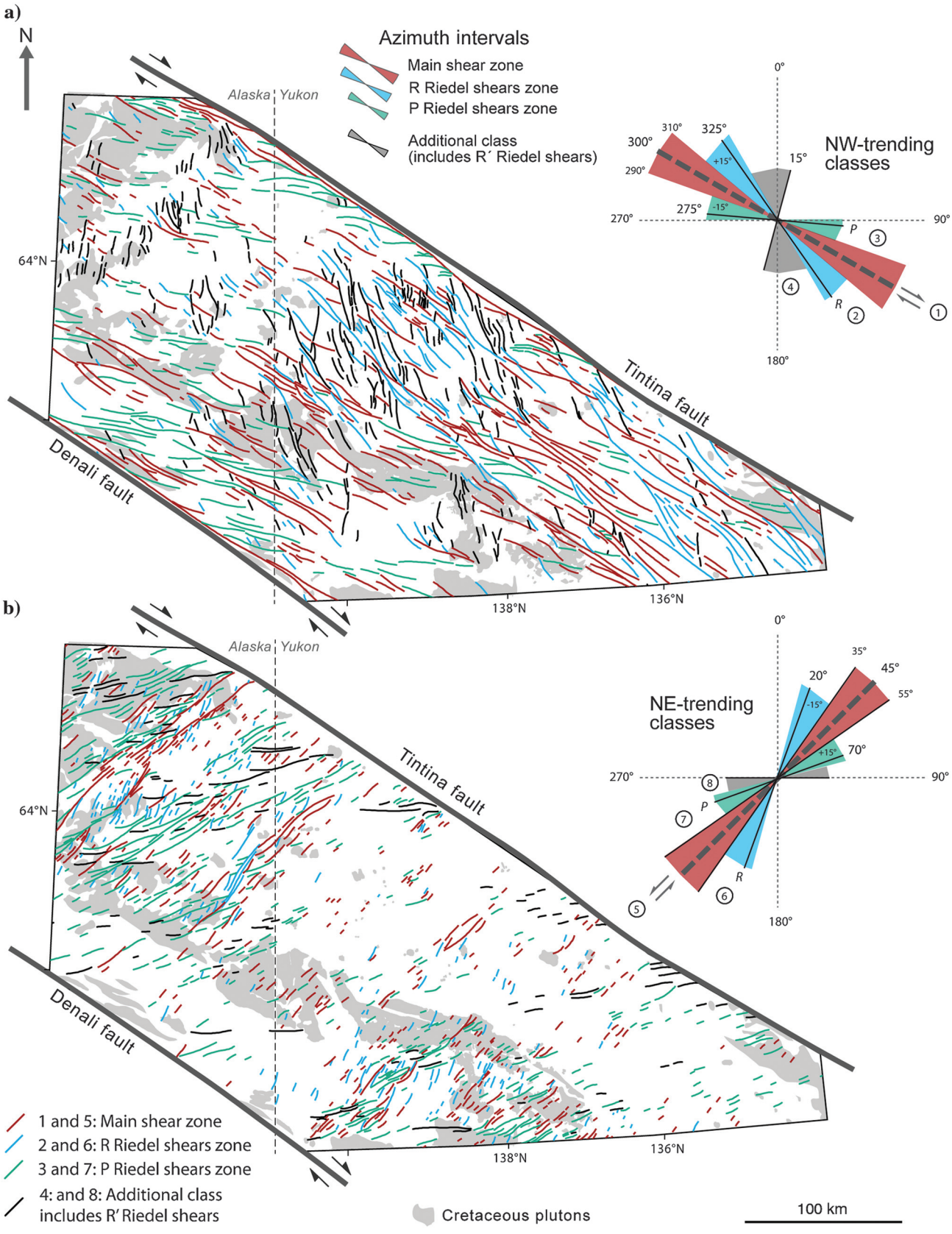

Figure 10. Structural interpretation of aeromagnetic lineament orientations assumed for dextral arc-parallel and sinistral arc-perpendicular magnetite-destructive strike-slip faults. Azimuthal classes are based on angular relations described for a Riedel shear model (Tchalenko, 1970). Map view and schematic orientation diagrams for (a) northwest-trending arrays and (b) northeast-trending arrays.

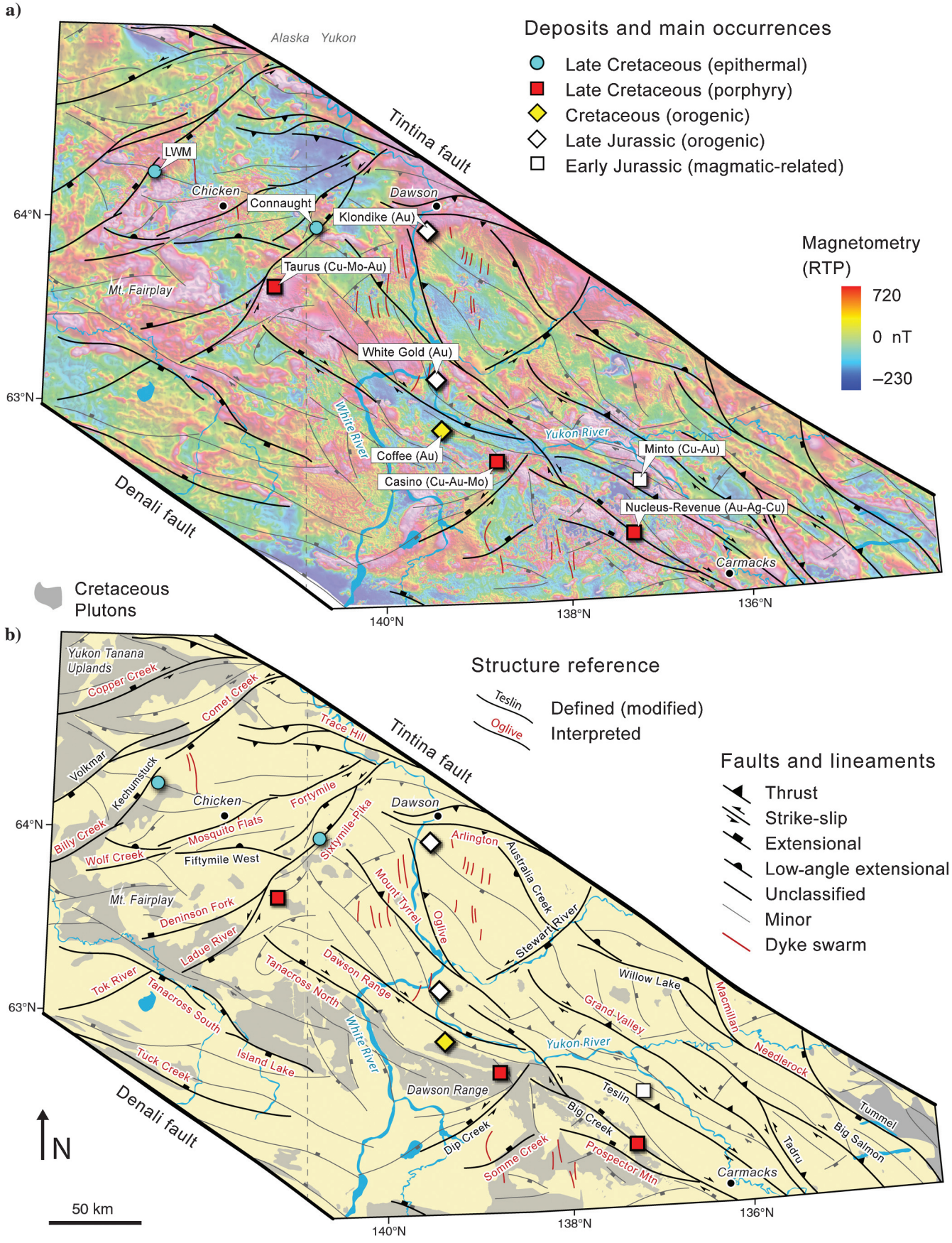

Figure 11. Simplified aeromagnetic lineament and magnetite-destructive fault system maps and the distribution of significant mineral deposits. (a) RTP magnetic map and (b) map of Cretaceous plutons and newly proposed and previously defined fault systems.

sion and the formation of a pull-apart basin (Figure 12). Subvolcanic stocks, hydrothermal breccias, and hydrofractures in this area are interpreted to have formed as a result of locally enhanced structural damage in this fault-relay zone and explain the position of known porphyry-related mineralization (Figures 12 and 13).

Northeast-trending fault systems

Seven major northeast-trending fault-fracture systems with highly continuous and linear patterns are identified and are best developed within the Alaskan portion of the study area. These aeromagnetic lineaments and discontinuities have strike lengths up to ~180 km (Figure 11) and may accommodate fault block rotations between major regional-scale dextral strike-slip systems such as the Kaltag, Iditarod-Nixon Fork, and Farewell faults (Figure 1; Page et al., 1995; Koehler, 2013). These discrete, linear, magnetite-destructive discontinuities are responsible for the apparent truncation of orogen- and arc-parallel aeromagnetic domains, as well as northwest-southeast elongated, high-amplitude anomalies. Examples of previously known northeast-trending faults with a strong magnetic signature at the study area are the Volkmar (Foster, 1976) and Kechumstuk faults in Alaska (Day et al., 2014) and the Dip Creek fault in Yukon (Figure 11; Templeman-Kluit, 1974; Johnston, 1999; Ryan et al., 2013).

Northeast-trending structural systems are highly continuous and linear in eastern Alaska but are more arcuate and segmented in western Yukon (Figure 10b; Sánchez et al., 2013). Structural offsets and block segmentation are evident in which northeast-trending lineaments and northwest-trending geologic units are compared. The most prominent magnetic truncations and offsets of high-amplitude anomalies are observed across the Alaskan-Yukon border of the study area (e.g., Sixtymile-Pika fault; Figure 11a). An outstanding example of along-strike block segmentation is given by the areal exposure of igneous rocks of the mid-Cretaceous Whitehorse plutonic suite in which offset by northeast-trending magnetite-destructive discontinuities (Figure 11b). In the Dawson Range (Figure 11), the northeast-oriented Dip Creek fault (Templeman-Kluit, 1974; Johnston, 1999; Ryan et al., 2013) is the most prominent orogen-perpendicular fault and magnetic truncation east of the Yukon-Alaska border (Figure 10b). We interpret this fault to extend for ~130 km from near the Denali fault to the northern flank of the Dawson Range, where it terminates immediately south of the Big Creek fault.

Implications for mineralization

The series of linear magnetic discontinuities extracted from geophysical data sets and interpreted in this study as steeply dipping faults are inferred to play a significant structural role in the formation of magmatic-hydrothermal mineralization in western Yukon and eastern Alaska. In several cases, these structures correlate with established examples of Cretaceous to early Cenozoic magmatism, hydrothermal alteration, and mineralization. The clearest example of a northwest-trending structure defining the distribution of Cretaceous magmatic-hydrothermal mineralization is the Big Creek fault (Figures 11 and 12). This structure correlates spatially with volumetrically minor rhyodacite to dacite porphyry dikes, stocks, and intrusive breccias of early Late Cretaceous age (~75 Ma) and associated porphyry Cu-Au-(Ag-Mo) and epithermal Au-Ag mineralization at the Revenue, Nucleus (Figure 13), and Cash deposits, as well as the Tad and Sonora Gulch prospects (Hart, 1997; Selby and Creaser, 2001; Bennett et al., 2010; Bineli Betsi and Bennett, 2010; Allan et al., 2013). The same magmatic suite is responsible for the >1-Gt Casino Cu-Au-Mo deposit in the Dawson Range (Selby and Creaser, 2001; Allan et al., 2013). As previously indicated, fault relay zones along the Big Creek fault system are viewed as especially important features controlling the local emplacement of magma, hydrothermal fluid flow, and mineralization through enhanced structural permeability. At least six gold deposits (i.e., Nucleus, Revenue, Stoddart, Augusta, Antoniuk, and Laforma) occur within a pull-apart fault block bound by two subparallel northwest-trending and overlapping fault segments (Figure 12). The rhombohedral geometry of this fault block is further defined by secondary north–northwest-trending faults interpreted as R Riedel shears with oblique dextral-extensional slip as a result of near north-directed shortening (Figure 12f).

The northeast-trending structures of Alaska correlate most closely with occurrences of latest Cretaceous (72–67 Ma) porphyry Mo (Cu-W) mineralization and Ag-rich, polymetallic epithermal vein, and carbonate-replacement systems (Figure 14; Allan et al., 2013). The clearest example of the regional fault control on these systems is the Kechumstuk fault of the Fortymile District of Alaska (Szumigala et al., 2003; Day et al., 2014), which defines the location of the 70.5-Ma Fish volcanogenic massive sulfide prospect (Ag, Cu, Pb, Zn) (Dusel-Bacon, 2007; Full Metal Minerals, 2012), Little Whiteman carbonate replacement prospect (Zn, Pb, Ag) (Siron et al, 2012) and the Mosquito porphyry Cu-Mo prospect, as well as of a series of additional prospects (Figure 14; Cox and Singer, 1986). The northeast- to north–northeast-trending Kechumstuck fault is interpreted to respond to nearly north-directed shortening, resulting in a sinistral strike-slip fault and secondary north-trending R Riedel shears (Figure 14e). Similarly, Ag-rich epithermal vein systems near the Yukon-Alaska border have a dominantly northeast strike that suggests a close structural relationship to the parent Sixtymile-Pika strike-slip fault system (Allan et al., 2013; M. Allan, personal communication, 2014).

Discussion

In areas of poor rock exposure, in which opportunities for geologic observation in the field are limited, data sets with regional coverage are clearly required

to build sensible geologic and structural interpretations (Gunn et al., 1997). However, it is critical to test these a priori interpretations in areas where geologic structures are well constrained by field observations. Here, we discuss the effectiveness of our fault interpretation methodology by comparing the results with previously mapped fault traces. Although fault traces on published geologic maps themselves have inherent uncertainty, they are the most appropriate proxy for faults with "real" geologic expression. Second, we present new structural interpretations for fault systems and discuss their metallogenic significance. At last, we provide some guidelines on the critical evaluation of lineament interpretations, in which insufficient geologic information exists for ground truthing.

Effectiveness of the method

The lineaments and lineament systems interpreted from aeromagnetic data in this study successfully delineated several previously published geologic faults

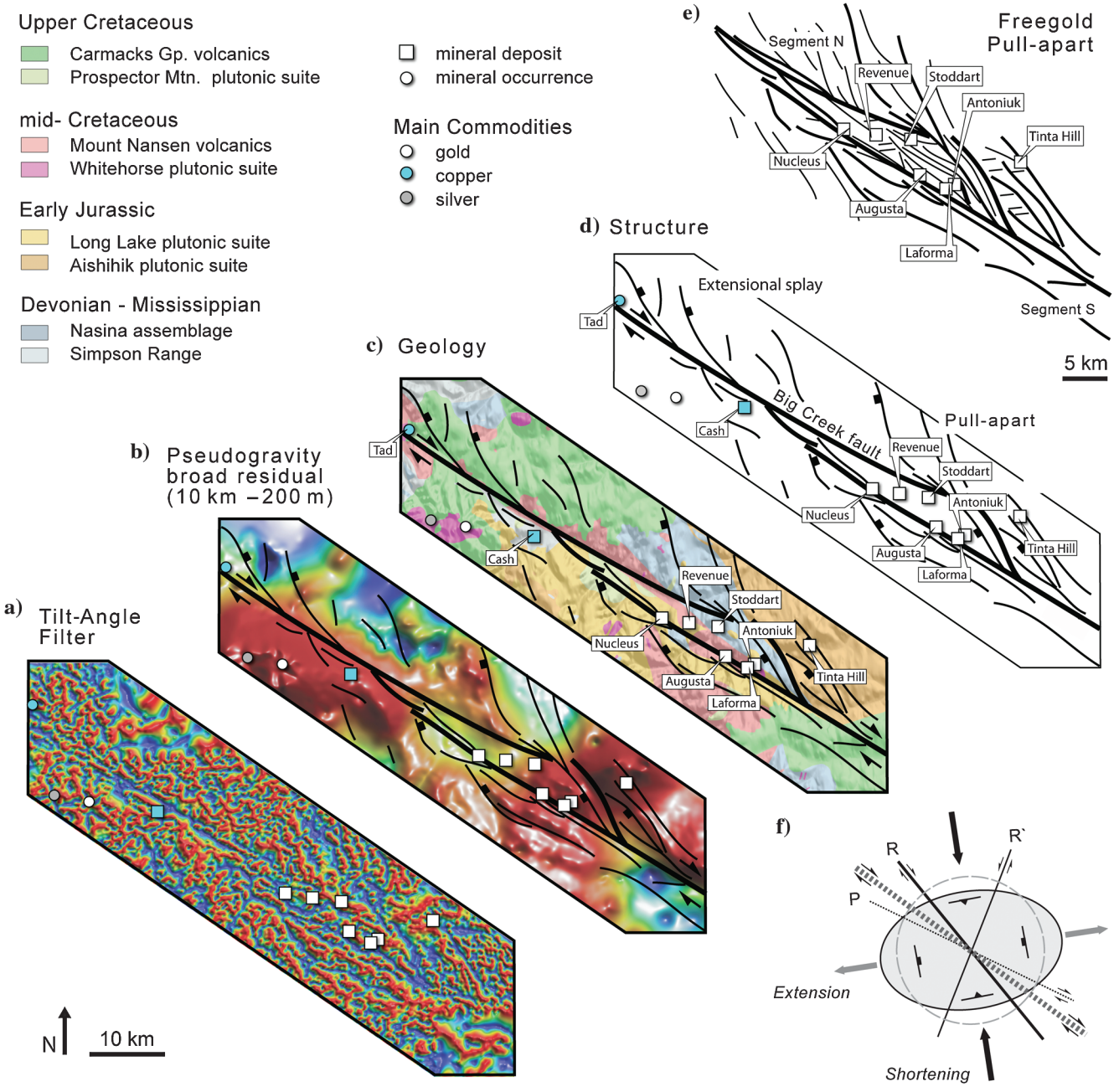

Figure 12. The northwest-trending magnetite-destructive Big Creek fault and associated mid- to Late Cretaceous magmatic-related mineral occurrences. (a) Tilt angle filter of the RTP magnetic grid, (b) pseudogravity residual (10 km–200 m) of the RTP magnetic grid, (c) compiled geologic map, (d) simplified structural interpretation, (e) structural array of the Freegold camp pull-apart, and (f) strain ellipsoid under near north-directed shortening and Riedel shears fault patterns for a northwest-trending dextral strike-slip main shear zone.

(Figure 4). These include the steep-dipping, northeast-trending Volkmar fault (Foster, 1976), Kechumstuk fault (Day et al., 2014), and Dip Creek fault (Templeman-Kluit, 1974; Ryan et al., 2013) and the moderately to steeply dipping northwest-trending Big Creek fault (Tempelman-Kluit, 1984), Big Salmon fault, and Tummel fault (Campbell and Wheeler, 1960) in Yukon. The success of the interpretation in highlighting these faults is primarily due to their easily recognized high-frequency and high-contrast expression in the aeromagnetic grids. Kinematic interpretations of these faults based on the offsets of geologic units and aeromagnetic domains are also consistent with previous field-based investigations. For example, the sinistral strike-slip displacements of the Copper Creek, Comet Creek, Sixtymile-Pika, and Dip Creek faults (Figure 11b) are consistent with displacements interpreted regionally for northeast-trending fault arrays in central and eastern Alaska (e.g., Page et al., 1995; Glen, 2004). Similarly, a dextral sense of displacement on the Big Creek fault is consistent with previous field map interpretations (Tempelman-Kluit, 1984; Ryan et al., 2013). For each of these geologic faults, the location of principal fault traces was improved and arrays of second-order fault segments, splays, and fault linkage zones (e.g., Freegold pull-apart; Figure 12) were interpreted.

The methodology was also effective in detecting several moderate- to shallow-angle faults (<50° dip), such as the northwest-trending Willow Lake detachment fault in Yukon (Ryan et al., 2010) and the Fiftymile fault in Yukon and Alaska (Figure 11; Foster et al., 1994; Mortensen, 1996). However, the methodology did not directly address the likely dip angle or sense of displacement on lower angle structures. Another limitation of the methodology is its inability to distinguish low-angle stratigraphic contacts from low-angle thrust or detachment surfaces.

An important goal of developing a systematic multidata set approach to fault interpretation was to recognize new fault systems with potential metallogenic significance and exploration potential. A significant result of this study is the delineation of the Sixtymile-Pika fault system — a ~150-km-long, northeast-trending strike-slip structure that controlled Late Cretaceous porphyry, skarn, and epithermal style mineralization (Allan et al., 2013; M. Allan, personal communication, 2014). Only short strike-length elements of the fault system were previously mapped (Foster, 1970; Plafker et al., 1994; Mortensen, 1996), but the integration of aeromagnetic, topographic, geologic, and gravity data strongly suggests that these are segments of a much larger fault system. An apparent ~17-km sinistral offset across this fault system is interpreted from offset geologic and magnetic markers and is supported by field kinematic evidence (M. Allan, personal communication, 2014).

Conversely, another important test of the fault interpretation is whether it failed to recognize any previously mapped or inferred structures. An apparent example is the northeast-trending, southeast-dipping Stewart River fault, a major inferred normal structure in west-central Yukon (Ryan et al., 2010), which juxtaposed amphibolite facies Paleozoic metamorphic rocks to the northwest against essentially undeformed and unmetamorphosed mid-Paleozoic volcanic rocks to the south (Staples et al., 2013). The most likely reason for the structure's weak aeromagnetic expression is the low magnetic contrast between the adjacent fault blocks (Figure 11). In addition, the position, curvature, and dip angle of this fault is currently poorly constrained. Regardless, we include this inferred structure in the simplified structural and geologic maps (Figures 11 and 15) due to the overwhelming geologic evidence for its existence.

Integration of geologic faults and new aeromagnetic lineaments

A general conclusion of this study is that the continuity of major geologic faults has been underestimated and that on average, fault systems have greater strike lengths than previously mapped (e.g., Figures 3a and 11b). A significant example in eastern Alaska is a linkage between the previously recognized Volkmar fault and the newly interpreted Comet Creek aeromagentic discontinuity (Figure 11). These two fault segments link along a major breached relay ramp generating a ~160-km-long northeast-trending and southeast-dipping sinistral-extensional fault system. Geologic map pattern interpretation supports that the Volkmar–Comet Creek fault system may be responsible for the footwall exhumation of mid-Cretaceous plutons northwest of the fault trace. Geologic and aeromagnetic domain offsets across the northeastern most Comet Creek fault support sinistral offsets of Cretaceous plutons and demonstrates post-mid-Cretaceous activity. Subparallel to the Volkmar fault, the Kechumstuck fault (Day et al., 2014) clearly links to the newly defined Billy Creek aeromagnetic discontinuity, which coincides with a short fault segment mapped by Foster (1970) (Figure 11b). Furthermore, to the northeast, the Kechumstuck fault trace appears to link to the Comet Creek fault through a narrow soft-linkage zone. Geologic map pattern interpretation supports the presence of a northeast-trending graben bound by the Billy Creek–Kechumstuck and Volkmar faults. Extension in this area may have accommodated Early Tertiary plutonism and the deposition and preservation of Paleocene to Eocene volcanic rocks (Figure 15). Early Tertiary intrusions and volcanic deposits, in addition to lateral offset of mid-Cretceous plutons, suggest Late Cretaceous to Early Tertiary fault activity, which is supported by apparent fault control of the Late Cretaceous Fish massive sulfide prospect (Ag, Cu, Pb, Zn), Little Whiteman carbonate replacement prospect (Zn, Pb, Ag), and Mosquito porphyry Cu-Mo prospect (Dusel-Bacon et al., 2009; Siron et al., 2010; Day et al., 2014).

The northwestern termination of the Teslin fault remains unresolved. In this study, the Teslin fault trace

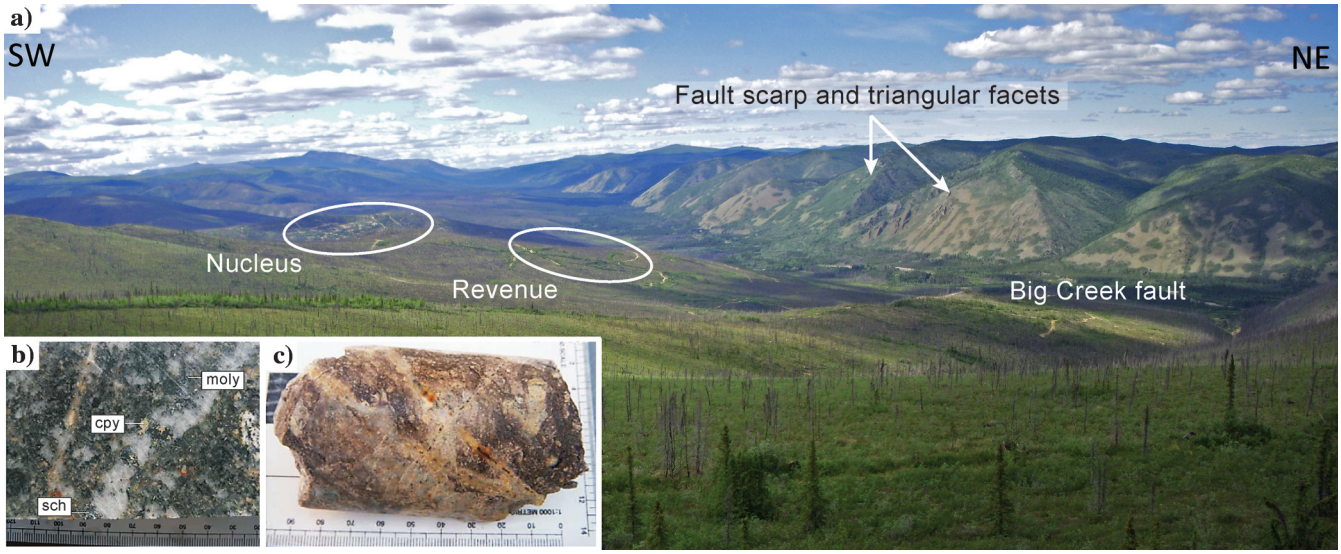

Figure 13. View of the Big Creek river valley and Nucleus and Revenue gold deposits. (a) Southwest-facing triangular facets are interpreted as a result of the Big-Creek fault scarp; (b and c) porphyry clast-dominated breccia from the Revenue deposit with molybdenite (moly), chalcopyrite (cpy), and scheelite (sch) mineralization. Average grades at the Revenue porphyry deposit are 0.34 g/t Au, 3.14 g/t Ag, 0.13% Cu, and 0.04% Mo (Northern Freegold, 2012b).

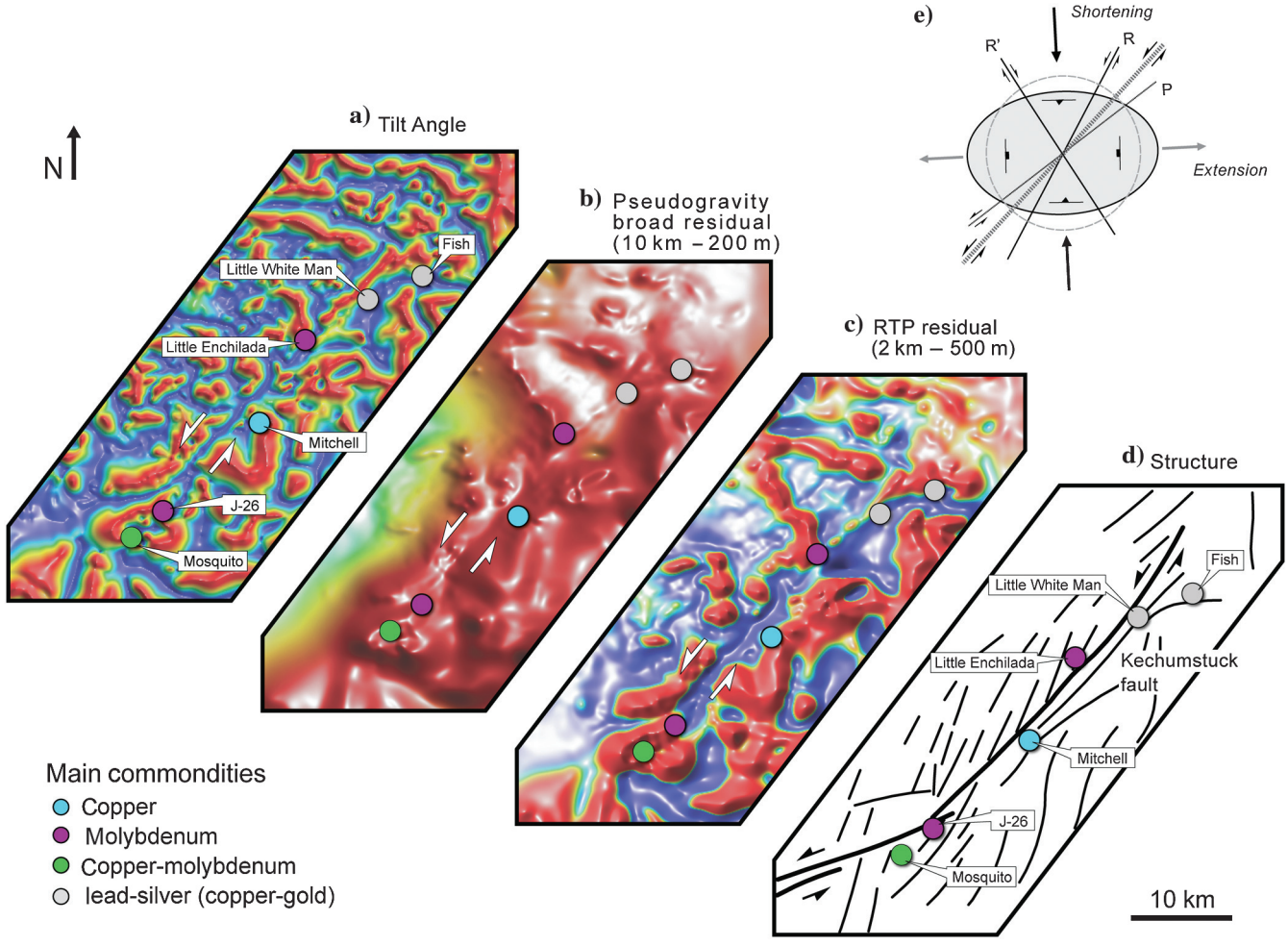

Figure 14. The northeast-trending, magnetite-destructive and associated Late Cretaceous mineral occurrences. (a) Tilt angle filter of the RTP magnetic grid, (b) pseudogravity residual (10 km–200 m) of the RTP magnetic grid, (c) RTP upward-continued residual (2 km–500 m) grid, (d) simplified structural array of the Kechumstuck fault, and (e) strain ellipsoid under near north-directed shortening and Riedel shears fault patterns for a northeast-trending sinistral strike-slip main shear zone.

(Gordey and Makepeace, 2003) is correlated with the northwest-oriented aeromagnetic discontinuity located immediately west of the Minto Cu-Au deposit and east of Carmacks (Figure 11). Although the aeromagnetic discontinuity associated with the Teslin fault appears to terminate immediately south of the Yukon River, three newly interpreted northwest-trending aeromagnetic lineaments may function as relay structures connecting the Teslin fault to the Mount Tyrrel aeromagnetic discontinuity. The Mount Tyrrel discontinuity extends for ~135 km to the Yukon-Alaska border and terminates in the immediate vicinity of the Sixtymile-Pika fault. A second major aeromagnetic discontinuity, the north–northwest-trending Ogilive structure splays from the Mount Tyrrel in the direction of Klondike gold district. A speculative possibility is that displacement on the Teslin fault was accommodated to the northwest by motion on these structures.

Structural geology guidelines

In addition to understanding of principles and limitations of aeromagnetic data collection (Nabighian et al., 2002), data processing (Luyendyk, 1997), signal filtering (Milligan and Gunn, 1997; Verduzco et al., 2004), and anomaly modeling (Gunn, 1997), a robust structural interpretation for mineral exploration targeting requires an understanding of fault mechanisms, architecture, and structural permeability (Sibson, 1977; Caine et al., 1996), as well as an appreciation for the magnetic response of common lithologies (Clark, 1997), structural types (Prieto, 2000), hydrothermal alteration assemblages (Airo, 2002), and ore environments (Grant, 1985; Gunn and Dentith, 1997). The critical interpretation and integration of geologic and geophysical data sets also requires that aeromagnetic lineament arrays are evaluated within appropriate regional-scale tectonic and structural frameworks (e.g., strike-slip fault inter-

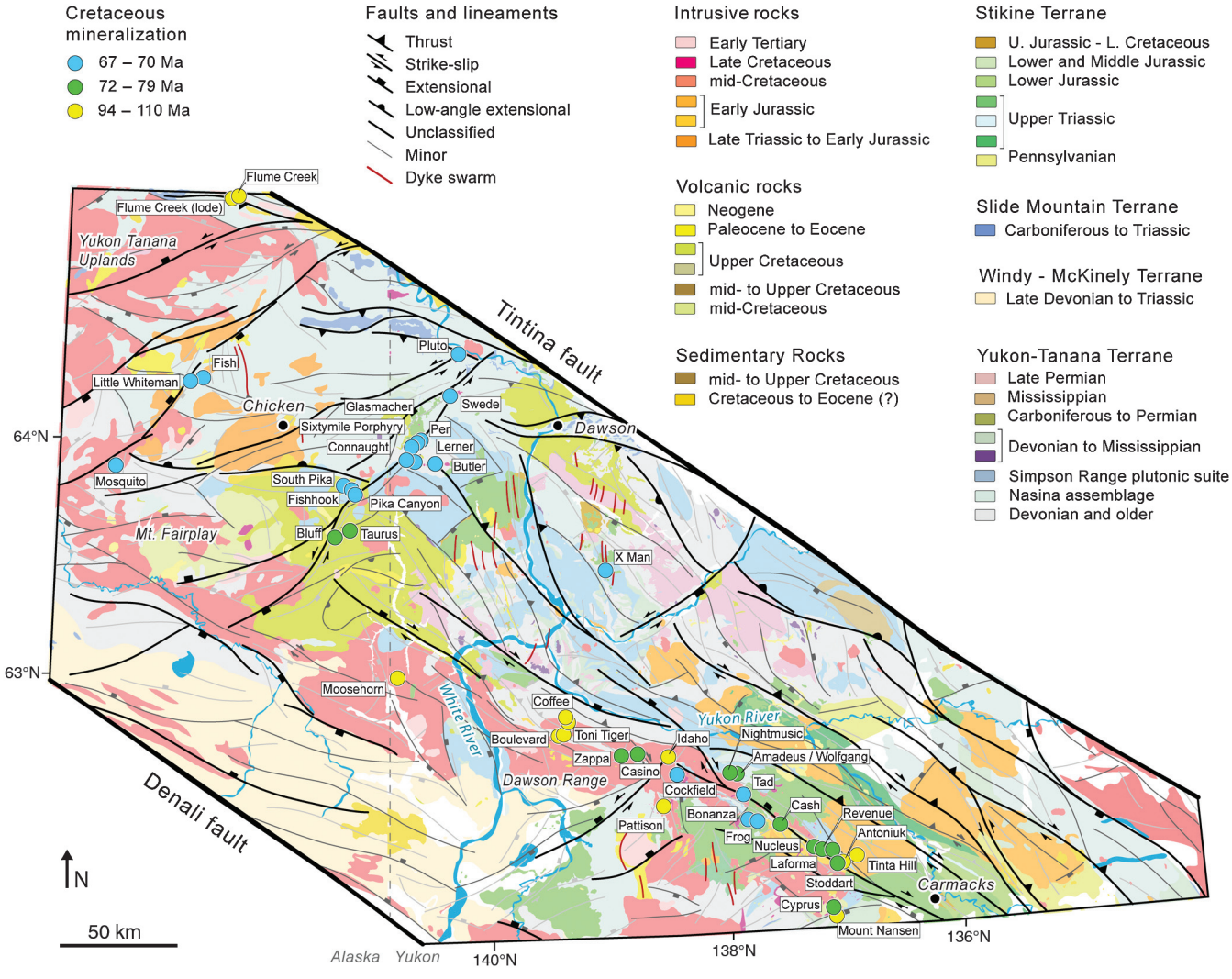

Figure 15. Simplified structural and geologic map showing regional fault systems (modified from Gordey and Ryan, 2005; Ryan et al., 2010; Beikman et al., 1980; Gordey and Makepeace, 2001; Sánchez, 2013), and the spatial distribution of significant mineral deposits and prospects of Cretaceous age (Allan et al., 2013).

pretations in the Oregon Cordillera (Blakely et al., 2000); buried normal faults in the Rio Grande Rift, New Mexico (Grauch et al., 2001); and thrust-related folding in the Canadian Northwest Territories (Nabighian et al., 2005). The use of appropriate tectonic and metallogenic frameworks is especially important for geophysical targeting of specific mineral deposit types (e.g., porphyry targeting in the Pebble porphyry district, Alaska; Anderson et al., 2013; Shah et al., 2013).

Conclusions

The methodology described in this paper provides a guideline for the systematic assessment of aeromagnetic lineaments as geologically meaningful structures by comparison with gravimetric, topographic, and geologic data sets. The multidata set-stacking procedure used is easily adapted for additional data layers or for alternative weighting schemes. Attributing lineaments with a reliability index provides a numerical basis for querying and filtering features with varying degrees of geologic significance. This offers a means of filtering out insignificant lineaments for more sophisticated structural interpretations.

Outcomes of the study relevant to future geoscientific and mineral exploration activities include

1) The recognition of 17 major fault systems in the western Yukon and eastern Alaska Cordillera, of which at least three (Big Creek, Sixtymile-Pika, and Kechumstuck faults) exert a known structural control on Cretaceous magmatism and hydrothermal mineralization. Previously, unrecognized fault systems and aeromagnetic features provide new targeting opportunities for mineral exploration in this region.
2) The eastern Alaska and western Yukon Cordillera is dissected by northeast- and northwest-trending aeromagnetic discontinuities that correlate with previously known and newly inferred geologic fault systems. Evidence for fault block segmentation is provided by (1) abrupt variations in the orientation of geologic contacts, (2) areal exposure of mid-Cretaceous igneous rocks of the Whitehorse plutonic suite, (3) sinistral and dextral strike-slip offsets of geologic units and aeromagnetic markers, and (4) the presence and offsets of geomorphologic trenches, ridges, and river systems.
3) The distribution of early Late Cretaceous (79–72 Ma) porphyry-epithermal systems in the Dawson Range of western Yukon supports a first-order structural control by northwest-trending dextral strike-slip structures (e.g., Big Creek fault).
4) The distribution of latest Cretaceous (72–67 Ma) porphyry-epithermal and carbonate-replacement style mineralization in eastern Alaska and far western Yukon supports a first-order structural control by northeast-trending sinistral strike-slip to oblique extensional structures (e.g., Kechumstuk and Sixtymile-Pika faults).
5) Second-order fault segments, splays, and fault linkage zones recognized in aeromagnetic and other data sets correlate locally with known magmatic-hydrothermal features and mineral occurrences (e.g., gold occurrence in the Freegold pull-apart). Recognizing such features in geophysical data is an obvious structural targeting criterion for mineral exploration.

Acknowledgments

This research has been supported by the Yukon Gold Project, a collaborative research venture between the Mineral Deposit Research Unit of The University of British Columbia and a consortium of industry participants, that include: Aldrin Resource Corp., Barrick Gold Corp., Full Metal Minerals Corp., Gold Fields Canada Exploration, Northern Freegold Resources Ltd., Kinross Gold Corp., Radius Gold, Inc., Silver Quest Resources Ltd., Taku Gold Corp., Teck Resources Ltd., and Underworld Resources, Inc. The project benefited from a Collaborative Research and Development grant from the Natural Science and Engineering Research Council of Canada, as well as a grant through the Geomapping for Energy & Minerals program of Natural Resources Canada. The authors are also grateful to the Yukon Geological Survey and the Geological Survey of Canada for their enormous support. The research also received significant funding from Natural Resources Canada and from the Natural Sciences and Engineering Research Council of Canada. We would like to sincerely thank all persons who shared inspiring ideas with us, including (but not limited to) M. Colpron, S. Israel, J. Ryan, W. Ciolkiewicz, D. MacKenzie, and T. Bissig. We would like to particularly acknowledge contributions made by D. Core and A. Buckingham of Fathom Geophysics LLC who compiled, leveled, and gridded the geophysical data sets. This contribution benefited greatly from thorough and insightful reviews by B. Morris and B. Drenth.

References

Airo, M. L., 2002, Aeromagnetic and aeroradiometric response to hydrothermal alteration: Surveys in Geophysics, **23**, 273–302.

Airo, M. L., and S. Mertanen, 2008, Magnetic signatures related to orogenic gold mineralization, Central Lapland Greenstone Belt, Finland: , **64**, 14–24, doi: 10.1016/j.jappgeo.2007.10.003.

Allan, M. M., J. K. Mortensen, C. J. R. Hart, L. A. Bailey, M. G. Sánchez, W. Ciolkiewicz, G. G. McKenzie, and R. A. Creaser, 2013, Magmatic and metallogenic framework of West-Central Yukon and Eastern Alaska, *in* M. Colpron, T. Bissig, B. Rusk, and J. Thompson, eds., Tectonics, metallogeny, and discovery: The North American Cordillera and similar accretionary settings: SEG, Special Publication, vol. 17, 111–168.

Allis, R. G., 1990, Geophysical anomalies over epithermal systems: Journal of Geochemical Exploration, **36**, 339–374, doi: 10.1016/0375-6742(90)90060-N.

Anderson, E. D., M. W. Hitzman, T. Monecke, P. A. Bedrosian, A. K. Shah, and K. D. Kelley, 2013, Geological analysis of aeromagnetic data from southwestern Alaska: Implications for exploration in the area of the Pebble porphyry Cu-Au-Mo deposit: Economic Geology, **108**, 421–436, doi: 10.2113/econgeo.108.3.421.

Arefi, H., and P. Reinartz, 2011, Accuracy enhancement of ASTER global digital elevation models using ICESat data: Remote Sensing, **3**, 1323–1343, doi: 10.3390/rs3071323.

Baker, T., and J. R. Lang, 2001, Fluid inclusion characteristics of intrusion-related gold mineralization, Tombstone-Tungsten magmatic belt, Yukon Territory, Canada: Mineralium Deposita, **36**, 563–582, doi: 10.1007/s001260100189.

Baranov, V., and H. Naudy, 1964, Numerical calculation of the formula of reduction to the magnetic pole: Geophysics, **29**, 67–79, doi: 10.1190/1.1439334.

Beikman, H. M., 1980, Geologic map of Alaska: U.S. Geological Survey, 1:2 500 000, 2 sheets.

Bennett, V., M. Colpron, and M. Burke, 2010, Current thinking on Dawson Range tectonics and metallogeny: Yukon Geological Survey, Miscellaneous report, 2–12.

Beranek, L. P., and J. K. Mortensen, 2011, A hinterland and foreland record of arc-continent collision: An example from the Late Permian Klondike orogeny, North American Cordillera: Tectonics, **30**, TC5017, doi: 10.1029/2010TC002849.

Bineli Betsi, T., and V. Bennett, 2010, New U-Pb age constraints at Freegold Mountain: Evidence for multiple phases of polymetallic mid- to Late Cretaceous mineralization, *in* K. E. MacFarlane, L. H. Weston, and L. R. Blackburn, eds., Yukon exploration and geology 2009: Yukon Geological Survey, 57–84.

Blakely, R. J., R. Wells, T. Tolan, M. Beeson, A. Trehu, and L. Liberty, 2000, New aeromagnetic data reveal large strike-slip (?) faults in the northern Willamette Valley, Oregon: Geological Society of America Bulletin, **112**, 1225–1233, doi: 10.1130/0016-7606(2000)112<1225:NADRLS>2.0.CO;2.

Burns, L. E., Fugro Airborne Surveys Corp., and Fugro GeoServices, Inc., 2011, Ladue survey area: Magnetic and electromagnetic line, grid, and vector data and maps, Fortymile mining district, Tanacross Quadrangle, eastern Alaska: Alaska Division of Geological & Geophysical Surveys Geophysical Report 2011-1, 26 sheets, 1 DVD, scale 1:63,360.

Burns, L. E., U. S. Bureau of Land Management, Fugro Airborne Surveys Corp., and Stevens Exploration Management Corp., 2008, Line, grid, and vector data, plot files, and descriptive project report for the airborne geophysical survey of part of the western Fortymile mining district, east-central Alaska: Alaska Division of Geological & Geophysical Surveys Geophysical Report 2008-1, 9 sheets, 1 DVD.

Caine, J. S., J. P. Evans, and C. B. Forster, 1996, Fault zone architecture and permeability structure: Geology, **24**, 1025–1028, doi: 10.1130/0091-7613(1996)024<1025:FZAAPS>2.3.CO;2.

Campbell, R. B., and J. O. Wheeler, 1960, Geology, Glenlyon, Yukon Territory: Geological Survey of Canada Map, Preliminary Series, vol. **13**, scale 1:253,440.

Canadian Geodetic Information System, 2012, Geoscience data repository, Geodetic Survey Division, Earth Sciences Sector, Natural Resources Canada, http://gdr.nrcan.gc.ca/gravity/can2k_iso_e.php, accessed 1 February 2012.

Clark, D., 1999, Magnetic petrology of igneous intrusions: Implications for exploration and magnetic interpretation: Exploration Geophysics, **30**, 5–26, doi: 10.1071/EG999005.

Clark, D., S. Geuna, and P. Schmidt, 2004, Predictive magnetic exploration models for porphyry, epithermal, and iron oxide copper-gold deposits: Implications for exploration: P700 Final Report, AMIRA International Ltd.

Clark, D. A., 1997, Magnetic petrophysics and magnetic petrology: Aids to geological interpretation of magnetic surveys: AGSO Journal of Australian Geology & Geophysics, **17**, 83–103.

Colpron, M., S. P. Gordey, G. W. Lowey, D. White, and S. J. Piercey, 2007b, Geology of the northern Whitehorse trough, Yukon (NTS 105E/12, 13, and parts of 11 and 14; 105L/4 and parts of 3 and 5; parts of 115H/9 and 16; 115I/1 and part of 8) (1: 150 000 scale): Yukon Geological Survey, Open File, 2007-6.

Colpron, M., and J. L. Nelson, 2011, A digital atlas of terranes for the northern Cordillera: BC Geological Survey, GeoFile, 2011-11.

Colpron, M., J. L. Nelson, and D. C. Murphy, 2007a, Northern Cordilleran terranes and their interactions through time: GSA Today, **17**, no. 4/5, 4–10, doi: 10.1130/GSAT01704-5A.1.

Connard, G. G., R. W. Saltus, P. L. Hill, L. Carlson, and B. Milicevic, 1999, Alaska Digital Aeromagnetic Database, http://pubs.usgs.gov/of/1999/ofr-99-0503/data/, accessed 1 February 2012.

Cook, F. A., R. M. Clowes, D. B. Snyder, A. J. van der Velden, K. W. Hall, P. Erdmer, and C. A. Evenchick, 2004, Precambrian crust beneath the Mesozoic northern Canadian Cordillera discovered by lithoprobe seismic reflection profiling: Tectonics, **23**, 1–28, doi: 10.1029/2002TC001412.

Cox, D. P., and D. A. Singer, eds., 1986, Mineral deposit models: U.S. Geological Survey, Bulletin 1693.

Crawford, B. L., P. G. Betts, and L. Aillères, 2010, An aeromagnetic approach to revealing buried basement structures and their role in the Proterozoic evolution of the Wernecke Inlier, Yukon Territory, Canada: Tectonophysics, **490**, 28–46, doi: 10.1016/j.tecto.2010.04.025.

Day, W. C., J. M. O'Neill, C. Dusel-Bacon, J. N. Aleinikoff, and C. R. Siron, 2014, Geologic map of the Kechumstuk fault zone in the Mount Veta area, Fortymile mining district, east-central Alaska (ver. 1.1), U.S. Geological Survey Scientific Investigations Map 3291, scale 1:63,360, 10.3133/sim3291, accessed 12 March 2014.

DGGS Staff, Geoterrex-Dighem, and Stevens Exploration Management Corp., 1999, CD-ROM containing profile and gridded data and section lines of the 1998 geophysical survey data for part of the Fortymile mining district, Alaska, southern Eagle and northern Tanacross quadrangles: Alaska Division of Geological and Geophysical Surveys, Public data file 99-9, 1 DVD.

Direen, N. G., and P. Lyons, 2007, Regional crustal setting of iron oxide Cu-Au mineral systems of the Olympic Dam region, South Australia: Insights from potential-field modeling: Economic Geology, **102**, 1397–1414, doi: 10.2113/gsecongeo.102.8.1397.

Domzalski, W., 1966, Importance of aeromagnetics in evaluation of structural control of mineralization: Geophysical Prospecting, **14**, 273–291, doi: 10.1111/j.1365-2478.1966.tb01761.x.

Dragoni, M., 1993, The brittle-ductile transition in tectonic boundary zones: Annals of Geophysics, **36**, 37–44, doi: 10.4401/ag-4282.

Dusel-Bacon, C., V. L. Hansen, and J. A. Scala, 1995, High-pressure amphibolite facies dynamic metamorphism and the Mesozoic tectonic evolution of an ancient continental margin, east-central Alaska: Journal of Metamorphic Geology, **13**, 9–24, doi: 10.1111/j.1525-1314.1995.tb00202.x.

Dusel-Bacon, C., M. J. Hopkins, J. K. Mortensen, S. Dashevsky, J. R. Bressler, and W. C. Day, 2006, Paleozoic tectonic and metallogenic evolution of the pericratonic rocks of east-central Alaska and adjacent Yukon, *in* M. Colpron, and J. Nelson, eds., Paleozoic evolution and metallogeny of Pericratonic Terranes at the ancient Pacific Margin of North America, Canadian and Alaskan Cordillera: Geological Association of Canada, Special paper 45, 25–74.

Dusel-Bacon, C., M. A. Lanphere, W. D. Sharp, P. W. Layer, and V. L. Hansen, 2002, Mesozoic thermal history and timing of structural events for the Yukon-Tanana Upland, east-central Alaska: 40Ar/39Ar data from metamorphic and plutonic rocks: Canadian Journal of Earth Sciences, **39**, 1013–1051, doi: 10.1139/e02-018.

Dusel-Bacon, C., J. F. Slack, J. N. Aleinikoff, and J. K. Mortensen, 2007, Mesozoic magmatism and base-metal mineralization in the Fortymile mining district, eastern Alaska: Initial results of petrographic, geochemical, and isotopic studies in the Mount Veta area: U.S. Geological Survey, Professional Paper 1760-A, pp. 50.

Dusel-Bacon, C., J. F. Slack, J. N. Aleinikoff, and J. K. Mortensen, 2009, Mesozoic magmatism and base-metal mineralization in the Fortymile mining district, eastern Alaska: Initial results of petrographic, geochemical, and isotopic studies in the Mount Veta area, *in* P. J. Haeussler, and J. P. Galloway, eds., Studies by the U.S. Geological Survey in Alaska, 2007: U.S. Geological Survey, Prof. paper 1760-A, 1–50.

ESRI, 2013, ArcMap 10.1: Environmental Systems Resource Institute (ESRI).

Foster, H. L., 1970, Reconnaissance geologic map of the Tanacross quadrangle, Alaska: U.S. Geological Survey: Miscellaneous Geologic Investigations Series, Map I-593, scale 1:250,000.

Foster, H. L., 1976, Geologic map of the Eagle quadrangle, Alaska: U.S. Geological Survey, Miscellaneous Investigations Series I–922, 1 sheet, scale 1:250,000.

Foster, H. L., T. E. Keith, and W. D. Menzie, 1994, Geology of the Yukon-Tanana area of east-central Alaska, *in* H. L. Foster, T. E. C. Keith, and W. D. Menzie, eds., The geology of North America, The geology of Alaska: The Geological Society of America, vol. **G-1**, 205–240.

Full Metal Minerals, 2012, Full metal discovers a second massive sulphide system at 40 Mile, full metal minerals on the Web, http://www.fullmetalminerals.com/380/, accessed 20 December 2012.

Gabrielse, H., 1985, Major dextral transcurrent displacements along the Northern Rocky Mountain Trench and related lineaments in north-central British Columbia: Geological Society of America Bulletin, **96**, 1–14, doi: 10.1130/0016-7606(1985)96<1:MDTDAT>2.0.CO;2.

Gabrielse, H., J. W. H. Monger, J. O. Wheeler, and C. J. Yorath, 1991, Part A: Morphogeological belts, tectonic assemblages and terranes: Chapter 2, *in* H. Gabrielse, and C. J. Yorath, eds., Geology of the Cordilleran Orogen in Canada: Geological Survey of Canada, Geology of Canada, no. 4, 15–28, (also Geological Society of America, The Geology of North America, v. G-2).

Gabrielse, H., D. C. Murphy, and J. K. Mortensen, 2006, Cretaceous and Cenozoic dextral orogen-parallel displacements, magmatism, and paleogeography, north-central Canadian Cordillera, *in* Haggart, J. W., R. J. Enkin, and J. W. H. Monger, eds., Paleogeography of the North American Cordillera, evidence for and against large-scale displacements: Geological Association of Canada, Special paper 46, 255–276.

Garrity, C. P., and D. R. Soller, 2009, Database of the geologic map of North America: Adapted from the map by J.C. Reed Jr. and others (2005): U.S. Geological Survey, Data Series 424, http://pubs.usgs.gov/ds/424/.

Geological Survey of Canada, 2012, Residual total magnetic field 200 m grid of Canada, http://gdr.nrcan.gc.ca/aeromag/can200m_e.php, accessed 1 February 2012.

Glen, J. M., 2004, A kinematic model for the southern Alaska orocline based on regional fault patterns, *in* A. J. Sussman, and A. B. Weil, eds., Orogenic curvature: Integrating paleomagnetic and structural analyses:

Geological Society of America Special paper 383, 161–172.

Goldstein, A. G., 1980, Magnetic susceptibility anisotropy of mylonites from the Lake Char mylonite zone, southeastern New England: Tectonophysics, **66**, 197–211, doi: 10.1016/0040-1951(80)90046-3.

Gordey, S. P., and A. J. Makepeace, 2001, Bedrock geology, Yukon Territory: Geological Survey of Canada, Open File 3754 and Exploration and Geological Services Division, Yukon Region, Indian and Northern Affairs Canada, Open File 2001-1, scale 1:1 000 000.

Gordey, S. P., and A. J. Makepeace, 2003, Yukon digital geology, v.2.0: Geological Survey of Canada, Open File 1749: Yukon Geological Survey, Open File 2003-9(D), 2 CD-ROMs.

Gordey, S. P., and J. J. Ryan, 2005, Geology, Stewart River Area (115 N, 115 O, and part of 115 J), Yukon Territory: Geological Survey of Canada, Open File 4970, 1:250,000.

Grant, F. S., 1985, Aeromagnetics, geology and ore environments, I. Magnetite in igneous, sedimentary and metamorphic rocks: An overview: Geoexploration, **23**, 303–333, doi: 10.1016/0016-7142(85)90001-8.

Grauch, V. J. S., and D. L. Campbell, 1984, Does draping aeromagnetic data reduce terrain-induced effects?: Geophysics, **49**, 75–80, doi: 10.1190/1.1441636.

Grauch, V. J. S., M. R. Hudson, and S. A. Minor, 2001, Aeromagnetic expression of faults that offset basin fill, Albuquerque basin, New Mexico: Geophysics, **66**, 707–720, doi: 10.1190/1.1444961.

Grybeck, D. J., 2008, Alaska resource data file, new and revised records version 1.5: U.S. Geological Survey, Open file report, 2008-1225.

Gunn, P., and M. Dentith, 1997, Magnetic responses associated with mineral deposits: AGSO Journal of Australian Geology and Geophysics, **17**, 145–158.

Gunn, P. J., 1997, Quantitative methods for interpreting aeromagnetic data: A subjective review: AGSO Journal of Australian Geology and Geophysics, **17**, 105–114.

Gunn, P. J., D. Maidment, and P. R. Milligan, 1997, Interpreting aeromagnetic data in areas of limited outcrop: AGSO Journal of Australian Geology and Geophysics, **17**, 175–186.

Hansen, V. L., and C. Dusel-Bacon, 1998, Structural and kinematic evolution of the Yukon-Tanana Upland tectonites, east-central Alaska — A record of late Paleozoic to Mesozoic crustal assembly: Geological Society of America Bulletin, **110**, 211–230, doi: 10.1130/0016-7606(1998)110<0211:SAKEOT>2.3.CO;2.

Hart, C. J. R., 1997, TAD — An unusual porphyry occurrence in the Dawson Range, Yukon: Exploration and Geological Services Division, Yukon, Indian, and Northern Affairs Canada, Yukon Exploration and Geology, 145–151.

Hart, C. J. R., R. J. Goldfarb, L. L. Lewis, and J. L. Mair, 2004a, The Northern Cordilleran Mid-Cretaceous plutonic province: Ilmenite/magnetite-series granitoids and intrusion-related mineralization: Resource Geology, **54**, 253–280, doi: 10.1111/j.1751-3928.2004.tb00206.x.

Hart, C. J. R., J. L. Mair, R. J. Goldfarb, and D. I. Groves, 2004b, Source and redox controls on metallogenic variations in intrusion-related ore systems, Tombstone-Tungsten Belt, Yukon Territory, Canada: Transactions of the Royal Society of Edinburgh, **95**, 339–356, doi: 10.1017/S0263593304000276.

Hayward, N., W. Miles, and D. Oneschuk, 2011, Geophysical series, regional geophysical compilation project, Yukon Plateau, Yukon, parts of NTS 105, 106, 115 and 116: Geological Survey of Canada, Open File 6840, 2 sheets, doi: 10.4095/288586.

Heiskanen, W. A., and H. Moritz, 1967, Physical geodesy: W. H. Freeman.

Henderson, J. R., and J. Broome, 1990, Geometry and kinematics of Wager shear zone interpreted from structural fabrics and magnetic data: Canadian Journal of Earth Sciences, **27**, 590–604, doi: 10.1139/e90-055.

Henley, R. W., and D. P. M. Adams, 1992, Strike-slip fault reactivation as a control on epithermal vein-style gold mineralization: Geology, **20**, 443–446, doi: 10.1130/0091-7613(1992)020<0443:SSFRAA>2.3.CO;2.

Hildenbrand, T. G., 1983, FFTFIL: A filtering program based on two-dimensional Fourier analysis: U.S. Geological Survey, Open-file report, 83-237.

Hildenbrand, T. G., B. Berger, R. C. Jachens, and S. Ludington, 2001, Utility of magnetic and gravity data in evaluating regional controls on mineralization: Examples from the western United States, Structural controls on ore genesis: Reviews in Economic Geology, **14**, 75–109.

Hoschke, T., 2001, Geophysical signatures of copper-gold porphyry and epithermal gold deposits, and implications for explorations: CODES ARC Centre of Excellence in Ore Deposits, University of Tasmania.

IOC, IHO and BODC, 2003, Centenary Edition of the GEBCO Digital Atlas, published on CD-ROM on behalf of the Intergovernmental Oceanographic Commission and the International Hydrographic Organization as part of the General Bathymetric Chart of the Oceans: British Oceanographic Data Centre, Liverpool.

Irvine, R. J., and M. J. Smith, 1990, Geophysical exploration for epithermal gold deposits: Journal of Geochemical Exploration, **36**, 375–412, doi: 10.1016/0375-6742(90)90061-E.

Isles, D., and L. Rankin, 2013, Geological interpretation of aeromagnetic data: ASEG, CSIRO Publishing.

Jacobsen, B. H., 1987, A case for upward continuation as a standard separation filter for potential-field maps: Geophysics, **52**, 1138–1148, doi: 10.1190/1.1442378.

Johnston, S. T., 1999, Large-scale coast-parallel displacements in the Cordillera: A granitic resolution to a paleomagnetic dilemma: Journal of Structural Geology, **21**, 1103–1108, doi: 10.1016/S0191-8141(99)00015-2.

Koehler, R. D., 2013, Quaternary faults and folds (QFF): Alaska Division of Geological and Geophysical Surveys, Digital Data Series 3, http://maps.dggs.alaska.gov/qff/.

Lapointe, P., B. A. Chomyn, W. A. Morris, and R. L. Coles, 1984, Significance of magnetic susceptibility measurements from the Lac du Bonnet Batholith, Manitoba, Canada: Geoexploration, **22**, 217–229, doi: 10.1016/0016-7142(84)90013-9.

Lapointe, P., W. A. Morris, and K. L. Harding, 1986, Interpretation of magnetic susceptibility: A new approach to geophysical evaluation of the degree of rock alteration: Canadian Journal of Earth Sciences, **23**, 393–401, doi: 10.1139/e86-041.

Latham, A. G., K. L. Harding, P. Lapointe, W. A. Morris, and S. J. Balch, 1989, On the lognormal distribution of oxides in igneous rocks, using magnetic susceptibility as a proxy for oxide mineral concentration: Geophysical Journal, **96**, 179–184, doi: 10.1111/j.1365-246X.1989.tb05259.x.

Logan, J. M., P. Schiarizza, L. C. Struik, C. Barnett, J. L. Nelson, P. Kowalczyk, F. Ferri, M. G. Mihalynuk, M. D. Thomas, P. Gammon, R. Lett, W. Jackaman, and T. Ferbey, 2010, Geoscience map 2010-1: Bedrock geology of the QUEST map area, central British Columbia: Geological Survey of Canada, Open file 6476.

Lund, K., 2008, Geometry of the Neoproterozoic and Paleozoic rift margin of western Laurentia: Implications for mineral deposit settings: Geosphere, **4**, 429–444, doi: 10.1130/GES00121.1.

Luyendyk, A. P. J., 1997, Processing of airborne magnetic data: AGSO Journal of Australian Geology and Geophysics, **17**, 31–38.

Maidment, D. W., G. M. Gibson, and J. W. Giddings, 2000, Regional structure and distribution of magnetite: Implications for the interpretation of aeromagnetic data in the Broken Hill region, New South Wales: Exploration Geophysics, **31**, 8–16, doi: 10.1071/EG00008.

Mair, J. L., C. J. R. Hart, and J. R. Stephens, 2006, Deformation history of the northwestern Selwyn Basin, Yukon, Canada: Implications for orogen evolution and mid-Cretaceous magmatism: Geological Society of America Bulletin, **118**, 304–323, doi: 10.1130/B25763.1.

McClay, K., and M. Bonora, 2001, Analog models of restraining stepovers in strike-slip fault systems: AAPG Bulletin, **85**, 233–260.

McMechan, M. E., 2012, Deep transverse basement structural control of mineral systems in the southeastern Canadian Cordillera, Geological Survey of Canada, Contribution 20110294: Canadian Journal of Earth Sciences, **49**, 693–708, doi: 10.1139/e2012-013.

Miller, M. L., D. C. Bradley, T. K. Bundtzen, and W. McClelland, 2002, Late Cretaceous through Cenozoic strike-slip tectonics of southwestern Alaska: The Journal of Geology, **110**, 247–270.

Milligan, P. R., and P. J. Gunn, 1997, Enhancement and presentation of airborne geophysical data: AGSO Journal of Australian Geology and Geophysics, **17**, 63–75.

Ministry of Economy, Trade, and Industry (METI) of Japan and the United States National Aeronautics and Space Administration (NASA), 2011, Advanced spaceborne thermal emission and reflection radiometer (ASTER) global digital elevation model (GDEM), **2**: http://reverb.echo.nasa.gov/reverb/, accessed 1 February 2012

Moll-Stalcup, E. J., 1994, Latest Cretaceous and Cenozoic magmatism in mainland Alaska, *in* G. Plafker, and H. C. Berg, eds., The geology of Alaska: Boulder, Colorado: Geological Society of America, Geology of North America, **G-1**, 589–619.

Morin, R. L., 2007, Alaska gravity data, http://geomaps.wr.usgs.gov/gump/people/morin/alaska/gravity/gravity.html, accessed 1 February 2012.

Mortensen, J., 1990, Geology and U-Pb geochronology of the Klondike district, west-central Yukon Territory: Canadian Journal of Earth Sciences, **27**, 903–914, doi: 10.1139/e90-093.

Mortensen, J. K., 1992, Pre-Mid-Mesozoic tectonic evolution of the Yukon-Tanana terrane, Yukon and Alaska: Tectonics, **11**, 836–853, doi: 10.1029/91TC01169.

Mortensen, J. K., 1996, Geological compilations maps of the northern Stewart River map area, Klondike and Sixtymile districts (115N/15, 16; 115O13,14 and parts of 115O/15,16): Indian and Northern Affairs Canada, Yukon Region, Open file 1996-1(G), p. 10, scale 1:50,000.

Mortensen, J. K., C. J. R. Hart, D. C. Murphy, and S. Heffernan, 2000, Temporal evolution of early and mid-Cretaceous magmatism in the Tintina Gold Belt: The Tintina Gold Belt: concepts, exploration and discoveries, *in*, T. L. Tucker, and M. T. Smith, eds., Vancouver, British Columbia and Yukon Chamber of Mines: Cordilleran Roundup, **2**, 49–57.

Murphy, D. C., 2009, New mineral exploration opportunities highlighted by new geoscience data, Stevenson Ridge and Northern Kluane Lake Areas, Southwestern Yukon: Geoscience Forum Posters: Yukon Geological Survey.

Nabighian, M. N., V. J. S. Grauch, R. O. Hansen, T. R. LaFehr, Y. Li, J. W. Peirce, J. D. Phillips, and M. E. Ruder, 2005, 75th anniversary: The historical development of the magnetic method in exploration: Geophysics, **70**, no. 6, 33ND–61ND, doi: 10.1190/1.2133785.

Nelson, J. L., M. Colpron, and S. Israel, 2013, The Cordillera of British Columbia, Yukon and Alaska: Tectonics and metallogeny: SEG, **17**, 53–110.

Nelson, J. L., M. Colpron, S. J. Piercey, C. Dusel-Bacon, D. C. Murphy, and C. F. Roots, 2006, Paleozoic tectonic and metallogenic evolution of the pericratonic terranes in Yukon, northern British Columbia and eastern Alaska, *in* M. Colpron, and J. L. Nelson, eds., Paleozoic evolution and metallogeny of Pericratonic Terranes at

the ancient Pacific Margin of North America, Canadian and Alaskan Cordillera: Geological Association of Canada, **45**, 323–360.

Northern Freegold, 2012a, Northern Freegold extends the Nucleus Gold Deposit, Northern Freegold Resources on the web, http://www.northernfreegold.com/s/NewsReleases.asp?ReportID=551882, accessed 20 December 2012.

Northern Freegold, 2012b, Northern Freegold files revenue deposit NI 43-101 technical report at Freegold Mountain, Northern Freegold Resources on the web, http://www.northernfreegold.com/s/NewsReleases.asp?ReportID=511840, accessed 20 December 2012.

O'Neill, M., W. C. Day, J. N. Aleinikoff, and R. W. Saltus, 2010, The Black Mountain tectonic zone-A reactivated northeast-trending crustal shear zone in the Yukon-Tanana Upland of East-Central Alaska, *in* Larry P. Gough, and Warren C. Day, eds., Chapter D of Recent U.S. Geological Survey Studies in the Tintina Gold Province, Alaska, United States, and Yukon, Canada — Results of a 5-Year Project: Scientific Investigations Report 2007–5289–D: U.S. Geological Survey.

Page, R. A., G. Plafker, and H. Pulpan, 1995, Block rotation in east-central Alaska: A framework for evaluating earthquake potential?: Geology, **23**, 629–632, doi: 10.1130/0091-7613(1995)023<0629:BRIECA>2.3.CO;2.

Pilkington, M., and R. W. Saltus, 2009, The Mackenzie River magnetic anomaly, Yukon and Northwest Territories, Canada — Evidence for Early Proterozoic magmatic arc crust at the edge of the North American craton: Tectonophysics, **478**, 78–86, doi: 10.1016/j.tecto.2008.09.006.

Pilkington, M., D. B. Snyder, and K. Hemant, 2006, Weakly magnetic crust in the Canadian Cordillera: Earth and Planetary Science Letters, **248**, 476–485, doi: 10.1016/j.epsl.2006.06.010.

Plafker, G., and H. C. Berg, 1994, Overview of the geology and tectonic evolution of Alaska, *in* G. Plafker, and H. C. Berg, eds., The geology of Alaska: Boulder, Colorado: Geological Society of America, Geology of North America, 989–1022

Plafker, G., L. M. Gilpin, and J. C. Lahr, 1994, Neotectonic map of Alaska, *in* G. Plafker, and H. C. Berg, eds., Geology of North America: Geological Society of America, 2 sheets, scale 1:2,500,000.

Prieto, C., 2000, Gravity/magnetic signatures of various geologic models-an exercise in pattern recognition, *in* R. I. Gibson, and P. S. Millegan, eds., Geologic applications of gravity and magnetics: Case histories, SEG, Geophysical Reference Series, **8**, 20–27.

Purucker, M. E., and D. A. Clark, 2011, Mapping and interpretation of the lithospheric magnetic field: *in* M. Mandea, and M. Kortea, eds., Geomagnetic Observations and Models: Springer, **5**, 311–337.

Richards, J. P., 2000, Lineaments revisited: SEG Newsletter, **42**, 14–20.

Roberts, D. E., and G. R. T. Hudson, 1983, The Olympic Dam copper-uranium-gold deposit, Roxby Downs, South Australia: Economic Geology, **78**, 799–822, doi: 10.2113/gsecongeo.78.5.799.

Ryan, J. J., M. Colpron, and N. Hayward, 2010, Geology, southwestern Mcquesten and parts of northern Carmacks, Yukon: Geological Survey of Canada, Canadian Geoscience Map 7 (preliminary version), 1:125,000.

Ryan, J. J., A. Zagorevski, S. P. Williams, C. Roots, W. Ciolkiewicz, N. Hayward, and J. B. Chapman, 2013, Geology, Stevenson Ridge (northeast part), Yukon: Geological Survey of Canada, Canadian Geoscience Map 116 (2nd ed., preliminary), scale 1:100,000, doi: 10.4095/292407.

Saltus, R. W., 2007, Matching magnetic trends and patterns across the Tintina fault, Alaska and Canada, Evidence for offset of about 490 kilometers, *in* L. P. Gough, and W. C. Day, eds., U. S. Recent Geological Survey studies in the Tintina Gold Province, Alaska, United States, and Yukon, Canada, results of a 5-year project: U.S. Geological Survey, Scientific Investigations Report, 2007-5289-C, 7.

Saltus, R. W., P. J. Brown, II, R. L. Morin, and P. L. Hill, 2008, 2006 compilation of Alaska gravity data and historical reports: U.S. Geological Survey, Digital Series, 264, CD-ROM.

Sánchez, M. G., M. M. Allan, C. J. R. Hart, and J. K. Mortensen, 2013, Orogen-perpendicular magnetic segmentation of the western Yukon and eastern Alaska cordilleran hinterland: Implications for structural control of mineralization, *in* K. E. MacFarlane, M. G. Nordling, and P. J. Sack, eds., Yukon exploration and geology 2012: Yukon Geological Survey, 133–146.

Sandrin, A., R. Berggren, and S. Å. Elming, 2007, Geophysical targeting of Fe-oxide Cu–(Au) deposits west of Kiruna, Sweden: Journal of Applied Geophysics, **61**, 92–101, doi: 10.1016/j.jappgeo.2006.05.002.

Selby, D., and R. A. Creaser, 2001, Late and mid-Cretaceous mineralization in the northern Canadian Cordillera: Constraints from Re-Os molybdenite dates: Economic Geology, **96**, 1461–1467, doi: 10.2113/gsecongeo.96.6.1461.

Shah, A. K., P. A. Bedrosian, E. D. Anderson, K. D. Kelley, and J. Lang, 2013, Integrated geophysical imaging of a concealed mineral deposit: A case study of the world-class Pebble porphyry deposit in southwestern Alaska: Geophysics, **78**, no. 5, B317–B328, doi: 10.1190/geo2013-0046.1.

Sibson, R. H., 1977, Fault rocks and fault mechanisms: Journal of the Geological Society, **133**, 191–213, doi: 10.1144/gsjgs.133.3.0191.

Simpson, R. W., R. C. Jachens, R. J. Blakely, and R. W. Saltus, 1986, A new isostatic residual gravity map of the conterminous United States with a discussion on the significance of isostatic residual anomalies: Journal

of Geophysical Research, **91**, 8348–8372, doi: 10.1029/JB091iB08p08348.
Siron, C. R., M. W. Hitzman, and R. McLeod, 2010, Geology of the Little Whiteman carbonate hosted replacement Zn-Pb-Ag-(Cu) Prospect, western Fortymile district, Alaska: SEG, Special Publication, **15**, 421–436.
Spector, A., 1985, Comment on "Statistical methods for interpreting aeromagnetic data by A. Spector and F.S. Grant": Geophysics, **50**, 2278.
Spector, A., and F. S. Grant, 1970, Statistical models for interpreting aeromagnetic data: Geophysics, **35**, 293–302, doi: 10.1190/1.1440092.
Spector, A., and F. S. Grant, 1975, Comments on "Two-dimensional power spectral analysis of aeromagnetic fields": Geophysical Prospecting, **23**, 391, doi: 10.1111/j.1365-2478.1975.tb01536.x.
Staples, R. D., H. D. Gibson, R. G. Berman, J. J. Ryan, and M. Colpron, 2013, A window into the Early to mid-Cretaceous infrastructure of the Yukon-Tanana terrane recorded in multi-stage garnet of west-central Yukon, Canada: Journal of Metamorphic Geology, **31**, 729–753, doi: 10.1111/jmg.12042.
Sylvester, A. G., 1988, Strike-slip faults: Geological Society of America Bulletin, **100**, 1666–1703, doi: 10.1130/0016-7606(1988)100<1666:SSF>2.3.CO;2.
Szumigala, D. J., R. A. Hughes, and R. H. Harris, 2003, Alaska mineral industry 2003: Division of Geological and Geophysical Survey, Fairbanks, Alaska, Special Report 58.
Szumigala, D. J., R. J. Newberry, M. B. Werdon, J. E. Athey, D. S. P. Stevens, R. L. Flynn, K. H. Clautice, and P. A. Craw, 2002, Geologic map of the Eagle A-1 Quadrangle, Fortymile mining district: Alaska Division of Geological and Geophysical Surveys, Preliminary interpretive report, 2002-1A, 1 sheet, scale 1:63,360.
Tachikawa, T., M. Kaku, A. Iwasaki, D. Gesch, M. Oimoen, Z. Zhang, D. Jeffrey, T. Krieger, B. Curtis, J. Haase, M. Abrams, R. Crippen, and C. Carabajal, 2011, ASTER global digital elevation model version 2 — Summary of validation results: ASTER GDEM Validation Team, http://www.jspacesystems.or.jp/ersdac/GDEM/ver2Validation/Summary_GDEM2_validation_report_final.pdf.
Tchalenko, J. S., 1970, Similarities between shear zones of different magnitudes: Geological Society of America Bulletin, **81**, 1625–1640, doi: 10.1130/0016-7606(1970)81[1625:SBSZOD]2.0.CO;2.
Tempelman-Kluit, D. J., 1974, Reconnaissance geology of Aishihik Lake, Snag and part of Stewart River map-areas, west-central Yukon (115A, 115F, 115G and 115K): Geological Survey of Canada, Paper 73-41, 97.
Tempelman-Kluit, D. J., 1984, Geology, Laberge (105E) and Carmacks (105I), Yukon Territory: Geological Survey of Canada, maps with legends, scale 1:250,000.
Verduzco, B., J. D. Fairhead, C. M. Green, and C. MacKenzie, 2004, New insights into magnetic derivatives for structural mapping: The Leading Edge, **23**, 116–119, doi: 10.1190/1.1651454.
White, D., M. Colpron, and G. Buffett, 2013, Seismic and geological constraints on the structure and hydrocarbon potential of the northern Whitehorse trough, Yukon, Canada: Bulletin of Canadian Petroleum Geology, **60**, 239–255, doi: 10.2113/gscpgbull.60.4.239.
Wilson, F. H., J. G. Smith, and N. Shew, 1985, Review of radiometric data from the Yukon crystalline terrane, Alaska and Yukon Territory: Canadian Journal of Earth Sciences, **22**, 1813–1817, doi: 10.1139/e85-192.
Wintsch, R. P., R. Christoffersen, and A. K. Kronenberg, 1995, Fluid-rock reaction weakening of fault zones: Journal of Geophysical Research, **100**, 13021–13032, doi: 10.1029/94JB02622.
Yukon MINFILE, 2010, Yukon MINFILE — A database of mineral occurrences: Yukon Geological Survey, http://data.geology.gov.yk.ca/, accessed 1 December 2012 to 1 June 2013.

Matias Sanchez received a B.S. in geology from the University of Concepcion of Chile and an M.S. in tectonics and a Ph.D. from the Fault Dynamics Group at Royal Holloway University of London. He also completed a postdoctoral fellowship with the Mineral Deposit Research Unit of the University of British Columbia. He has more than 12 years of experience providing technical expertise in the areas of structural geology, magnetic data interpretation, and GIS for the mineral exploration industry and economic geology research projects. He has carried out detailed studies and fieldwork for the understanding of structural and tectonic controls of epithermal and porphyry style deposits in western Turkey, the Canadian Cordillera, southern Argentina, and Chile.

Murray Allan has been studying the metallogeny of the Yukon and Alaska Cordillera as an MDRU research associate since 2010. Previously, he carried out grassroots exploration with Anglo American in Brazil, Quebec, Utah, and Alaska. His Ph.D. research at the University of Leeds focused on the development of fluid inclusion analysis by laser ablation ICP-MS, and application of this technique to magmatic-hydrothermal gold deposits. He is currently applying his experience with hydrothermal fluid chemistry to regional metallogenic problems in the Northern Cordillera. He is a registered professional geoscientist with APEGBC.

Craig Hart received a B.S. (1986) from McMaster University, an M.S. (1995) from the University of British Columbia, and a degree (2005) from the University of Western Australia. He is the director of Mineral Deposit Research Unit at the University of British Columbia where he initiates and facilitates a wide range of mineral exploration industry-sponsored research projects focused on gold and porphyry systems, regional metallogeny, and exploration methods in orogenic belts. He previously worked as a senior research fellow at the Centre for Exploration Targeting at the University of Western Australia in Perth where he pursued research gold metallogeny of China and Mongolia. His early career was with the Yukon Geological Survey where he undertook regional mapping and metallogenic surveys in the northern Cordillera. He played a significant role in developing intrusion-related gold models, and understanding redox controls on regional metallogeny.

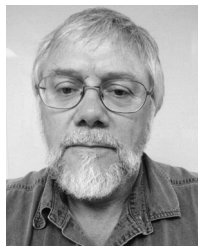

James Mortensen received a B.A.Sc. (1977) and M.A.Sc. (1979) from the University of British Columbia and a Ph.D. (1983) from the University of California, Santa Barbara. He has more than 40 years of field experience focused on regional tectonic and metallogenic studies in various orogenic belts (northern Cordillera, Yanshanian belt in northeast China, Guerrero Terrane in Mexico, Lhasa Block in Tibet, Otago Schist Belt in New Zealand, Mt Read Belt in Tasmania, and the Variscan Belt in Spain and Portugal), as well as the Canadian Shield. His main expertise is on orogenic and intrusion-related gold and VHMS deposits, and on the application of geochronology and radiogenic isotopes in tectonic and mineral deposit research. He had spent seven years as a research scientist with the Geological Survey of Canada in Ottawa, and since 1992, he has been a faculty member at the University of British Columbia, where he and his research group continue to investigate the geology and metallogeny of orogenic belts.